Design and UV writing of advanced Bragg gratings in optical fibers

Plougmann, Nikolai; Kristensen, Martin

Publication date:
2004

Document Version
Publisher's PDF, also known as Version of record

Ph.D. Thesis

Design and UV writing of advanced Bragg gratings in optical fibers

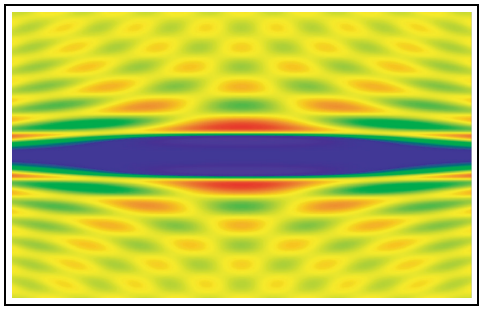

Nikolai Plougmann

COM
Technical University of Denmark
Kongens Lyngby, Denmark
April, 2004

Abstract

English abstract

Photosensitivity in germanium doped optical fibers has found its important and useful application in inscribing Bragg gratings since its discovery in 1978. The refractive index of germano-silica glasses changes (normally increases) during exposure to ultraviolet (UV) light. Illuminating an optical fiber with a UV laser that makes an interference pattern on the surface of the fiber, it is possible to induce a periodic change in the effective refractive index of the fiber, hereby inscribing a Bragg grating in it.

Two main contributions of this Ph.D. project are described below.

- Development of a novel polarization control method for UV writing of advanced Bragg gratings with arbitrary refractive index modulation profile including multiple π phase shifts. This method represents a practical cost-efficient technique that allows inscribing Bragg grating with any arbitrary apodization profile.
- Development of a novel efficient technique for Bragg grating design. The technique allows calculating an index modulation profile that should be inscribed in an optical fiber (or any other waveguide) in order to achieve a desired target spectrum of the grating. It is based on Marquardt-Levenberg algorithm of least-square optimization. The developed technique wins over all existing methods in computer time necessary for its implementation (only a couple of minutes of CPU time for a typical run on an average computer). Even more importantly, it has the remarkable ability to restrict some of the characteristics of the target grating, thus enabling, for example, the design of chirp-free gratings that are easy and cheap to fabricate with existing techniques, including the above mentioned polarization control method. In contrast, most other existing techniques produce complex grating designs with complicated chirp characteristics that are difficult, expensive and sometimes impossible to fabricate.

Dansk resumé

Siden sin opdagelse i 1978 er fotofølsomhed i germaniumdopede optiske fibre blevet brugt til det vigtige og nyttige formål, at skrive Bragg gitre. Brydningsindeks af germano-silica glas ændres (normalt forøges) ved udsættelse for ultraviolet (UV) lys. Ved bestråling af en optisk fiber med en UV laser som skaber et interferensmøster på fibrens overflade, er det muligt at inducere en periodisk ændring i fibrens effektive brydningsindeks, og derved skrive et Bragg gitter i fibren.

To af dette Ph.D. projekts afgørende bidrag er beskrevet efterfølgende.

- Udvikling af en ny polarisationskontrolmetode for UV skrivning af avancerede Bragg gitre med arbitrær brydningsindeksprofil med flere π faseskift. Denne metode repræsenterer en praktisk og relativt billig teknik som muliggør skrivning af Bragg gitre med hvilken som helst given apodiseringsprofil .

- Udvikling af en ny teknik til design af Bragg gitre. Denne teknik tillader beregningen af an indeksmodulationsprofil, som skal indskrives i en optisk fiber (eller en anden bølgeleder) for at opnå gitrets ønskede spektrum. Den er baseret på en Marquardt-Levenberg algoritme og er hurtigere end alle andre eksisterende metoder. Men hvad er endnu vigtigere, giver den mulighed for at fastholde bestemte egenskaber af designede gitre fra starten, hvorved det for eksempel bliver muligt at designe gitre uden chirp, som er nemme og billige at fabrikere med eksisterende teknologier, inklusivt ovenfor nævnte polarisationskontrolmetode. De fleste andre eksisterende teknikker, skaber derimod indviklede gitter designs med kompliceret chirp, som er svært og dyrt (eller ligefrem umuligt) at producere.

Publication list

[1] N. Plougmann and M. Kristensen. Efficient iterative technique for designing Bragg gratings. *Optics Letters*, 29(1):23–25, 2004.

[2] J.B.D. Jensen, N. Plougmann, H.-J. Deyerl, P. Varming, J. Hübner, and M. Kristensen. Polarization control method for ultraviolet writing of advanced Bragg gratings. *Optics Letters*, 27(12):1004–1006, 2002.

[3] M. Kristensen, J. Arentoft, J.B.D. Jensen, H.-J. Deyerl, J. Lægsgaard, C.-J. Marckmann, N. Plougmann, Y. Ren, S. Søgaard, and P. Varming. Bragg gratings and poling. *DOPS-NYT*, 16(2):49–54, 2001.

[4] H.-J. Deyerl, N. Plougmann, J.B.D. Jensen, F. Floreani, H.R. Sørensen, and M. Kristensen. Fabrication of advanced Bragg gratings with complex apodization profiles using the polarization control method. *Applied Optics - LP*, 2003. (Accepted March 2004).

[5] H.-J. Deyerl, N. Plougmann, F. Floreani, B. Zsigri, C. Peucheret, S.J. Hewlett, and M. Kristensen. A compact low dispersion fiber Bragg grating with high detuning tolerance for advanced modulation formats. *Optics Communication*, 2004. (Submitted).

[6] N. Plougmann, M. Kristensen, and H.-J. Deyerl. New iterative approach for designing Bragg gratings. In *BGPP, paper MD17*, Monterey, California, USA, 2003.

[7] F. Floreani, H.-J. Deyerl, N. Plougmann, H. Ou, J.B.D. Jensen, and M. Kristensen. A flexible approach for the apodization of planar waveguide Bragg gratings. In *BGPP, paper MD15*, Monterey, California, USA, 2003.

[8] H.-J. Deyerl, H.R. Sørensen, J.B.D. Jensen, N. Plougmann, and M. Kristensen. Fabrication and stability of fiber Bragg gratings for WDM applications using a 266 nm cw-laser. In *CLEO/QELS, paper CtuI2*, Baltimore, Maryland, USA, 2003.

[9] H.-J. Deyerl, N. Plougmann, J.B.D. Jensen, J. El-Bez, H.R. Sørensen, C. Peucheret, and M. Kristensen. Low-dispersion fiber Bragg gratings

written using the polarization control method. In *ECOC, paper 7.2.7*, Copenhagen, Denmark, 2002.

[10] H.-J. Deyerl, N. Plougmann, J.B.D. Jensen, H.R. Sørensen, and M. Kristensen. Polarization control method for UV writing of advanced Bragg gratings. In *IEEE/LEOS WFOPC*, pages 86–91, Glasgow, Scotland, 2002.

[11] J.B.D. Jensen, N. Plougmann, H.-J. Deyerl, and M. Kristensen. Polarization controlled UV writing of Bragg gratings. In *OFC, paper TuQ4*, pages 111–113, Anaheim, California, USA, 2002.

[12] N. Plougmann, J.B.D. Jensen, H.-J. Deyerl, H.R. Sørensen, and M. Kristensen. Polarization controlled UV writing of Bragg gratings. In *POWAG, paper WA3*, St. Petersburg, 2002.

[13] P. Varming, J.B.D. Jensen, N. Plougmann, M. Kristensen, and J. Hübner. New method for fabrication of advanced UV written Bragg gratings. In *BGPP 2001, paper BWA5*, Stresa, Italy, 2001.

Chapter 1

Introduction

Since the the first time a *fiber Bragg grating* (FBG) was inscribed in a Ge-doped fiber by Hill et al. in 1978 [1], FBGs have become widely used components in optical communication and sensor applications [2–7]. FBGs are used as low-cost, fiber compatible bandpass filters in wavelength division multiplexing (WDM) systems, for compensation of chromatic dispersion or for gain equalization [8,9]. Precise control over the spectral characteristics, e.g. the amplitude and phase response is required for the FBG when applied in optical networks [10]. To achieve high bandwidth utilization and high data rate in a WDM system, the frequency response of a FBG should have a rectangular amplitude spectrum and a linear phase response.

This chapter is an introduction to the thesis. It explains the basic concepts used throughout the thesis for those readers who may not be acquainted with the field of *fiber optics*. The topics it deals with are *optical fiber*, *Bragg grating* and *phase mask*.

1.1 Optical fiber

Optical fiber is a cylindrical dielectric waveguide. It is schematically illustrated in Fig. 1.1. It is made of silica (glass) doped with different chemical elements such as Ge, P [11], S and other. It has a cylindrical shape along its length z and its radius R is typically equal to 40 or $62.5\,\mu\text{m}$. It consists of a *core* with radius a and refractive index n_{core} and *cladding* with refractive index $n_{\text{clad}} < n_{\text{core}}$. This kind of fiber design represents a *step index fiber*. It is characterized by constant values a, R, n_{core} and n_{clad}. In general the parameters n_{core} and n_{clad} can be rather complicated functions of the distance from the center of the fiber depending on the fibers' applications. Some examples can be found in [12, 13]. The step index profiles will be used throughout this thesis.

In general the *Maxwell's equations* (3.1-1) need to be solved in order to describe propagation of electromagnetic waves through optical fibers. Wave-

lengths of light used in optical communication systems lies around 1.55 or 1.30 µm which is comparable to fiber's core radius. This implies that the *geometrical optics* approximation cannot be used, and general Maxwell's equations have to be solved. Nevertheless even in this case one can use geometrical optics to explain that light will propagate through the fiber due to the *total internal reflection* of light at the border of the core and the cladding. Light rays that fall at this border at angle greater then $\Phi = \arcsin\left(n_{\text{clad}}/n_{\text{core}}\right)$ will experience total reflection and will hereby propagate along the fiber.

Light propagating through the fiber can be described by the effective refractive index n_{eff} which be accurately defined in Chap. 3 in equation (3.1-18). In general the following inequality is fulfilled:

$$n_{\text{clad}} < n_{\text{eff}} < n_{\text{core}}.$$

1.2 Fiber Bragg grating

A *fiber Bragg grating* (FBG) represents a periodic change in the effective refractive index of the fiber n_{eff} as a function of the distance z along the fiber:

$$n_{\text{eff}}(z) = n_0 + n_{\text{eff}}^{\text{ave}}(z) + n_{\text{eff}}^{\text{mod}}(z) \cdot \mathrm{G}\left[\frac{2\pi}{\Lambda(z)} z + \varphi(z)\right], \tag{1.2-1}$$

where n_0 is the unperturbed effective refractive index of the fiber without the Bragg grating, $n_{\text{eff}}^{\text{ave}}(z)$ describes change of the average refractive index along the grating. Function $\Lambda(z)$ is grating's period at z and $\mathrm{G}(t)$ is a periodic function with period 2π. Functions $n_{\text{eff}}^{\text{mod}}(z)$ and $\varphi(z)$ are connected directly to such characteristics of the grating as its *apodization* (or *modulation strength*) and *chirp* respectively. All four mentioned functions $n_{\text{eff}}^{\text{mod}}(z)$, $n_{\text{eff}}^{\text{ave}}(z)$, $\Lambda(z)$ and $\varphi(z)$ are slowly varying functions of z if compared to the period of the grating at a given point z.

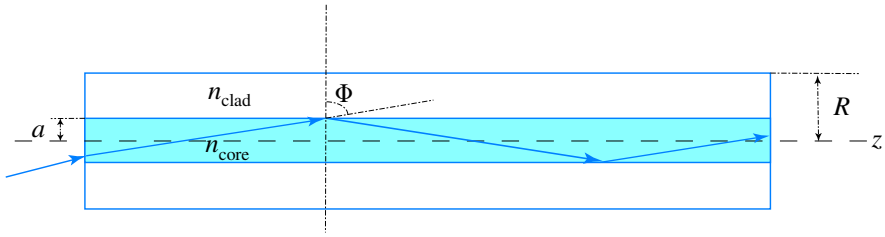

Figure 1.1: *A schematic drawing of an optical fiber.*

In Fig. 1.2 one can see a schematic drawing of a Bragg grating. The figure shows a dependency of the effective refractive index of the fiber as a function of the distance z along the grating. The apodization $n_{\text{eff}}^{\text{mod}}(z)$ is the envelope of the refractive index modulation, while average refractive index $n_{\text{eff}}^{\text{ave}}(z)$ is the effective refractive index averaged over a period of the grating $\Lambda(z)$ at the given position z along the grating.

It is common to assume $\mathrm{G}(t) = 2\cos(t)$. The dependency of the grating's period on z can be formally eliminated if its change along the grating $\Delta\Lambda$ ($\Delta\Lambda \ll \Lambda$) is much smaller than Λ by including this dependency into $\varphi(z)$. According to this, equation (1.2-1) can be rewritten in the following form:

$$\frac{n_{\text{eff}}(z)}{n_0} = 1 + \sigma(z) + 2\,\kappa(z)\cdot\cos\left[\!\left[\frac{2\pi}{\Lambda}z + \varphi(z)\right]\!\right], \tag{1.2-2}$$

where

$$\begin{cases} \sigma(z) \equiv n_{\text{eff}}^{\text{ave}}(z)\big/ n_0, \\ \kappa(z) \equiv n_{\text{eff}}^{\text{mod}}(z)\big/ n_0. \end{cases} \tag{1.2-3}$$

Chapter 3 of this thesis is dedicated to Bragg grating theory. But even now based only on general physical considerations, one can conclude that a fiber Bragg grating will function as a reflector of light with wavelength in the vicinity of a certain *Bragg wavelength* λ_0 with corresponds to a double optical path between two maxima (or minima) of the refractive index modulation:

$$\lambda_0 = 2n_0\Lambda. \tag{1.2-4}$$

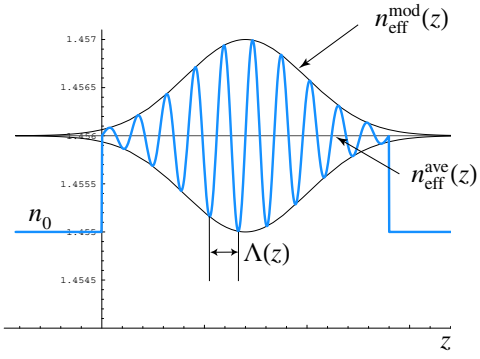

Figure 1.2: *A schematic drawing of a Bragg grating.*

The *Bragg vector* $\vec{K}$ of the grating is directed normally to the grating planes and its magnitude is equal to $K \equiv \left|\vec{K}\right| = 2\pi/\Lambda$. So the grating scatters light with wavevector $\vec{k}_1$ in a direction $\vec{k}_2$ given by $\vec{k}_2 = \vec{k}_1 - \vec{K}$. The condition for strong coupling between counter propagating directions $\left(\vec{k}_2 = -\vec{k}_1\right)$ gives the condition

$$k_0 \equiv \left|\vec{k}_1\right| = \left|\vec{k}_2\right| = \frac{K}{2} = \frac{\pi}{\Lambda}, \tag{1.2-5}$$

which is equivalent to the equation (1.2-4).

1.3 Phase mask

Fiber Bragg gratings are normally induced by illuminating a fiber with a doped core by UV radiation. The most common core dopant that makes silica photosensitive is germanium. This thesis deals only with Ge based photosensitivity of optical fibers discovered back in 1978 by Hill al. [1] If the fiber is illuminated with UV light that has a periodic intensity structure, a periodic change in refractive index of the doped core of the fiber will be induced, hereby producing a periodic change in its effective refractive index, i.e. a Bragg grating. The most common used technique for writing Bragg gratings in optical fibers is based on the *holographic method* [14, 15] using a *phase mask* [4].

Phase masks for UV-writing are made of silica with an etched surface as schematically shown in Fig. 1.3. The depth of the profile h is chosen in such a way that there is no *zero order* light propagation, i.e. the phase difference between light propagating in and between the ripples is equal to π times an odd integer number m:

$$h\,(n_{\text{silica}} - n_{\text{air}}) = k\,\frac{\lambda_{\text{UV}}}{2}, \quad k = 1, 3, 5\ldots \tag{1.3-1}$$

where n_{silica} and n_{air} are refractive indices of silica and air correspondingly and λ_{UV} is the wavelength of the UV light.

The diffraction angles Ψ_m are determined by

$$\sin\Psi_m = \frac{m\,\lambda_{\text{UV}}}{\Lambda_{\text{mask}}} + \sin\epsilon, \quad m = \pm1, \pm2, \pm3\ldots \tag{1.3-2}$$

where Λ_{mask} is phase mask's pitch period and ϵ is the falling angle of the incident UV light.

Generally, phase masks are designed in such a way that the only diffraction orders of significance are the first orders of diffraction, i.e. $m = \pm1$. This means that most of the power of the incident UV light is shared between the two first diffraction orders, thus making it possible to produce a good quality interference pattern after the phase mask. The produced UV interference pattern is then used to inscribe Bragg gratings.

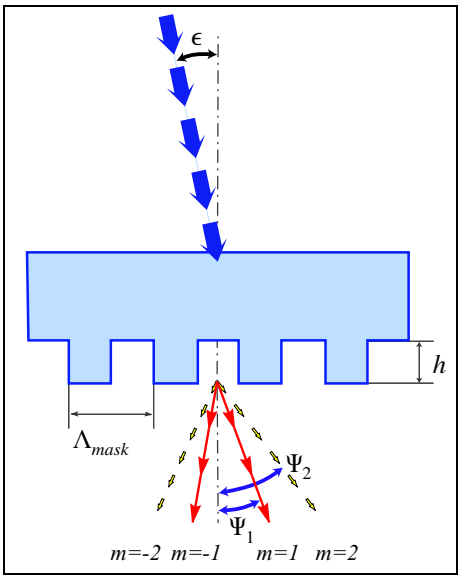

Figure 1.3: *Phase mask diffraction.*

Using equation (1.3-2) for $\epsilon = 0$ we get the half-angle ϕ between the diffraction orders $m = 1$ and $m = -1$ to be

$$\sin\phi = \frac{\lambda_{UV}}{\Lambda_{mask}},$$

so that the period of interference pattern created by the two orders $(m = \pm 1)$ is equal to

$$\Lambda = \frac{\lambda_{UV}}{2\sin\phi} = \frac{\lambda_{UV}}{2\ \lambda_{UV}/\Lambda_{mask}},$$

or

$$\Lambda = \Lambda_{mask}/2. \tag{1.3-3}$$

Equation (1.3-3) allows to rewrite equation (1.2-5) as

$$\boxed{k_0 = \frac{2\pi}{\Lambda_{mask}},} \tag{1.3-4}$$

while equation (1.2-4) becomes

$$\boxed{\lambda_0 = n_0\Lambda_{mask}.} \tag{1.3-5}$$

It can be convenient to write equations (1.2-1) and (1.2-2) using dimensionless variable

$$\zeta \equiv k_0 z, \tag{1.3-6}$$

where k_0 is defined by equations (1.2-5) and (1.3-4). So we have

$$\frac{n_{\text{eff}}(\zeta)}{n_0} = 1 + \sigma(\zeta) + 2\,\kappa(\zeta) \cdot \cos\left[2\zeta + \varphi(\zeta)\right], \tag{1.3-7}$$

and in the general case

$$\frac{n_{\text{eff}}(\zeta)}{n_0} = 1 + \sigma(\zeta) + \kappa(\zeta) \cdot \mathrm{G}\left[2\zeta + \varphi(\zeta)\right]. \tag{1.3-8}$$

1.3.1 Linearly chirped phase mask

In a case of a *chirped* phase mask we have $\Lambda_{\text{mask}} = \Lambda_{\text{mask}}(z) = \Lambda_{\text{mask}}(\zeta)$. Normally the change of the phase mask period $\Delta\Lambda$ along its length z (or ζ) is much smaller then Λ_{mask}. In this case one can formally consider Λ_{mask} as constant and include the distance dependency into an additional term $\varphi(\zeta)$. As an example let us consider a *linearly-chirped phase mask* of length L with dependency

$$\Lambda_{\text{mask}}(z) = \Lambda_0 + cz,$$

where Λ_0 is the phase mask period in its center, c is its chirp and z is the coordinate along the fiber length $0 \leqq z \leqq L$. The constants c, L and Λ_0 must satisfy the following inequality:

$$\frac{c \cdot L}{\Lambda_0} \ll 1. \tag{1.3-9}$$

The phase in equations (1.3-7) and (1.3-8) can be written as:

$$2\zeta = 2k_0 z = \frac{4\pi}{\Lambda_{\text{mask}}(z)}\, z = \frac{4\pi}{\Lambda_0 + cz}\, z = \frac{4\pi}{\Lambda_0}\left(1 + \frac{c}{\Lambda_0}\, z\right)^{-1} z.$$

Using that fact that the chirp in the phase mask is small which is given by the equation (1.3-9), we can rewrite the equation above in the following form:

$$2\zeta = \approx \frac{4\pi}{\Lambda_0}\, z - \frac{4\pi c}{\Lambda_0^2}\, z^2.$$

Thus, an effective additional phase $\varphi(z)$ in this case will look like:

$$\varphi(z) = -\frac{4\pi c}{\Lambda_0^2}\, z^2.$$

Returning back to $\zeta \equiv k_0 z$ we have the following expression for $\varphi(\zeta)$:

$$\varphi(\zeta) = -\frac{2^2\pi^2 c}{\pi\Lambda_0^2} z^2 = -\left(\frac{2\pi}{\Lambda_0}\right)^2 z^2 \frac{c}{\pi} = -k_0^2 z^2 \frac{c}{\pi},$$

and finally

$$\boxed{\varphi(\zeta) = -\frac{c}{\pi}\zeta^2.} \tag{1.3-10}$$

The calculations above show that it is possible to disregard the change of the phase mask's period and assume it to be constant, but instead one can introduce an additional effective phase $\varphi(\zeta)$ in the grating given by equation (1.3-10).

Chapter 2

Photosensitivity in germanium-doped silica

UV writing of Bragg gratings in Ge-doped optical fibers has an important commercial application in the field of telecommunication and optical sensors. However, the fundamental understanding of the UV-induced processes in silica glasses is still far from being satisfactory. There exist two different classes of models that try to explain the UV induced photosensitivity.

- ➢ *Microscopic models* that are based on the assumption that defects formed in the glass materials lead to the change of its refractive index [16–20],
- ➢ *Macroscopic models* assume that the refractive index changes are based on the macroscopic effects in the glass such as *compaction* or *stress* [21–24].

2.1 Background

Silica is a frozen-in undercooled liquid with no higher order symmetry [25]. The majority of the silicon atoms are bound to four oxygen atoms in perturbed tetrahedral structures, with oxygen atoms bound to two neighboring silicon atoms. Since the germanium atoms have the same number of valent electrons, they can occupy silicon place without disrupting the geometry of the glass structure. When germanium doped silica glass is fabricated under oxygen deficient conditions, a large variety of *defects* are formed in the glass matrix. Most of the UV photosensitivity models rely on these defects to absorb the UV light with the wavelength close to 242 nm where the absorption is strongest. Strong *singlet-singlet transitions* at 180 nm and 242 nm and a weaker *singlet-triplet transition* at 325 nm are connected with germanium related defect centers [26].

While the macroscopic models determine the change in the refractive index through the compaction, stress and corresponding volume change, the microscopic models assume that creation of different defects such as so-called GeE' centers [27, 28] change the refractive index of the silica glass according to the *Kramers-Kronig relation* [29]:

$$\Delta n(\lambda) = \frac{1}{2\pi^2} \int_0^\infty \frac{\Delta\alpha(\lambda')\, d\lambda'}{1 - (\lambda'/\lambda)^2}. \tag{2.1-1}$$

In the equation (2.1-1) above $\int$ means the principal value of the integral and $\Delta\alpha(\lambda)$ and $\Delta n(\lambda)$ are the changes in the *absorption coefficient* of the material and its refractive index respectively as functions of the wavelength λ. A large number of defects have been identified using theoretical speculations and spectroscopy. Nevertheless, no satisfactory quantitative agreement with the experimental results has been achieved for those microscopic models that are based on the Kramers-Kronig relation.

Despite that in some cases good qualitative agreement with the experimental data has been found for the macroscopic models, they lack the ability to describe the fundamental physical phenomena that lead to the refractive index change. Thus it is desirable to have a comprehensive microscopic model in order to understand the physical reasons for photosensitivity and be able to describe it both quantitatively and qualitatively.

2.2 Dipole-quadrupole model

Recently a principally new type of a microscopic model has been developed by Martin Kristensen, COM, Technical University of Denmark [30, 31]. Its innovative original idea is to disregard the origin and the internal structure of the germanium related defects, but to take the energy levels and transitions between them into consideration. In this way one does not care about what the defects actually are and how they give rise to the refractive index change through the Kramers-Kronig relation (2.1-1). This makes an advantageous background for the theoretical calculations: the number of all thinkable defects is very large and they are hard to identify, while the energy levels of the UV absorption spectrum in the germano-silica glasses are unambiguous and well studied. The model describes UV writing near 242 nm, the influence of hydrogen loading, and the thermal erasure in germanium-doped silica. In addition it gives an explanation of many spectroscopic observations during and after UV irradiation.

The model is based on the assumption that germanium sites in the glass work as gates for the transfer of energy from the light to the glass matrix. When a germanium site has absorbed a photon, the energy may be transferred

to other sites in the glass, leading to rearrangement of the local structure. The energy transfer happens predominantly through *dipole-quadrupole* transitions, leading to an r^{-8} dependence of the transition probability as a function of the distance r from the germanium site [32, 33], which gives the name to the model. In addition, some multiphoton processes are possible using the excited germanium-site state as intermediate level. It is assumed that two different metastable defect states are formed in the silica matrix. One of these is possibly identical to the triplet state identified through *ab initio* calculations by Sulimov et al. [34] Formation of the first type of defect in the glass increases the refractive index because it is situated higher in the band gap, bringing its fundamental transitions closer to visible wavelengths. On the other hand, formation of other defects with very small overlap integrals reduces the refractive index, since transitions from these states to more normal electronic glass states are forbidden.

The most basic assumption of the model is that energy is initially absorbed in close vicinity of the germanium atoms and later transferred to other sites in the glass where defects are created. The 242 nm absorption is strong for oxygen-deficient germanium-doped silica due to so-called *germanium-related oxygen-deficient centers* (GODC) and very weak or absent for fully oxidized silica [35]. Most UV writing uses wavelengths near the 242 nm absorption [4, 6].

In Fig. 2.1-(a) a simple energy level scheme for germanium sites is shown. The model assumes that two metastable defect sites with long lifetimes exist in the glass. One of these defects is responsible for positive index changes and is referred to as a D_1 defect in Fig. 2.1-(b). Another defect denoted D_2 in Fig. 2.1-(c) accounts for negative refractive index changes. It is assumed that a UV photon excites a GODC defect from its ground state $^1S_0$ to its excited state $^1S_1$. By a *dipole-quadrupole transition* a nearby site in the silica matrix is excited into a D_1^*, wherefrom it falls into a metastable state D_1 through a *non-radiative decay* with significant structural rearrangements. In order to return to the original glass matrix configuration and annihilate the photoinduced index change, structural rearrangements are required, thus giving D_1 virtually infinite lifetime at normal conditions. Thermal excitation is necessary to return the glass matrix to its original state and hereby remove the refractive index change.

Another metastable state D_2 is generated during further exposure. It may be a result of further rearrangement of D_1 defect, which would explain that the negative index change is preceded by a positive index change. The D_2 defect may absorb another UV photon and be excited into the band gap. This process is speeded up by the presence of the *hydrogen* molecules since their *singlet-triplet transition* coincides with the energy of the D_2 state plus the energy of the UV photon as shown in Fig. 2.1-(c). As a result, hydrogen and deuterium will catalyze the elimination of the index reducing defect. The effect is greatly enhanced by heating which excites the molecules to their first vibration level and effectively reduces the H_2 singlet-triplet transition energy to 11.5 eV.

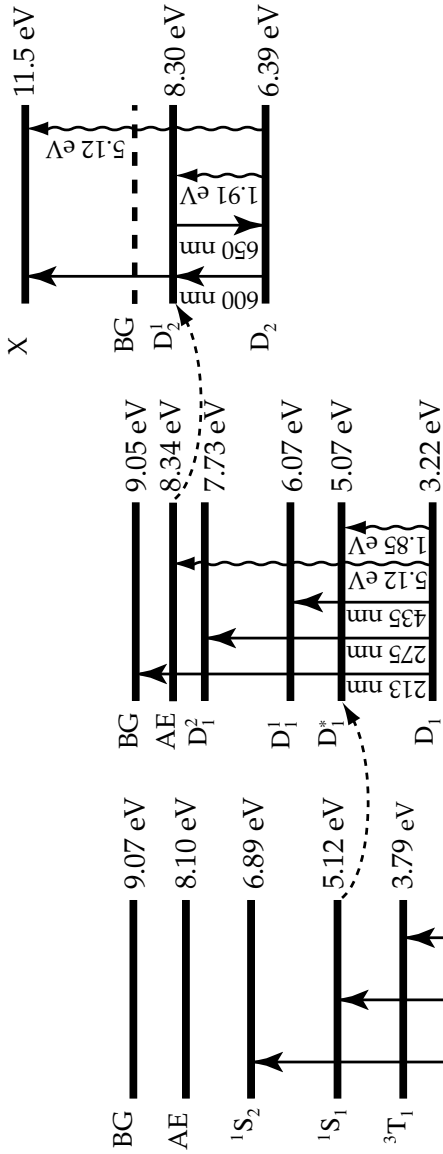

Figure 2.1: *Energy level scheme for germanium sites* (GODC) *and the defects* D_1 *and* D_2 *involved in the UV-induced processes in silica glass. Optical transitions are drawn as vertical lines, non-radiative transitions are labelled as vertical zigzag lines. "AE" stands for absorption edges, "BG" – band gap energies and the ground state "GS". "X" is a state localized above the band gap and resonant with the singlet-triplet transition energy in the hydrogen molecule.*

Hydrogen loading is presumed to catalyze the absorption both because of the presence of a nearby OH transition [36] and because it may modify the germanium sites in such a way that they become oxygen deficient [37] and increase the 242 nm transition probability. Both these catalytic effects may demand initial activation and therefore be facilitated by heat treatment.

If one denotes the concentration of the index increasing defects D_1 as x and the concentration of the index decreasing defects D_2 as y, one can write the rate equations for the defect concentrations x and y assuming that $y \ll x < 1$

$$\begin{cases} \dfrac{dx}{dt} = c_1(1-x) - c_2 x, \\ \dfrac{dy}{dx} = c_3 x - c_4 y, \end{cases} \tag{2.2-1}$$

where t is time and parameters c_1, c_2, c_3 and c_4 are rather complicated functions of the UV laser wavelength and intensity, hydrogen loading pressure, decay rate for the allowed optical transition and the distance r from the nearest germanium atom [30,31].

With initial conditions $x(0) = 0$ and $y(0) = 0$ one can solve the rate equations (2.2-1) and find x and y as functions of t and r. The UV induced refractive index change is calculated by integrating over the germanium molar volume while it is assumed that the distribution of germanium atoms is equidistant. The resulting index change Δn is given by an equation which looks like

$$\Delta n(t) \propto \int_0^{r_{\max}} \left[\Delta n^x_{\max} x(t,r) + \Delta n^y_{\max} y(t,r)\right] \rho(r) r^2 dr. \tag{2.2-2}$$

In the last equation (2.2-2) $\Delta n^x_{\max}$ is the index change induced by unit density of index increasing defects and $\Delta n^y_{\max}$ is the index change induced by unit density of index decreasing defects. In the model they are assumed to be equal to 0.04 and -0.1 respectively. The value of $r_{\max}$ is the radius of the GODC "unit cell" and $\rho(r)$ is a the *radial density function* of germanium atoms, determined from experimental X-ray diffraction data for silica [38].

2.3 Summary

To my knowledge, the *dipole-quadrupole model* is one of a few microscopic models which give satisfactory qualitative and quantitative description of the UV photosensitivity in germano-silica glasses. Nevertheless, my personal opinion is that a large number of introduced parameters (over 20) make the model difficult to comprehend and obscure its physical meaning. On the other

side, the large number of parameters give hope that the model and its predictive ability can be improved significantly if more work is done on adjusting them. I feel that especially those parameters that describe hydrogen (and deuterium) loading need a lot of hard work of adjustment. While the theory provides excellent description of the photosensitivity in fibers without H_2 loading [30,31], I never succeeded in getting satisfactory coincidence between the model and the experimental results for the loaded fibers. Possible explanation for this fact could be that UV writing is very sensitive to hydrogen loading and depends on the concentration of the hydrogen (or deuterium) in the fiber's core. However, one can never be sure how large the concentration of hydrogen is in the core of the fiber. Partly because there are no direct easy methods of its measurement and partly because it changes all the time during the UV exposure due to its out-diffusion. Fig. 2.2 shows an example of a 5 mm long uniform grating written in D_2 loaded HNLF fiber (section 4.4). The discrepancy can be also partly explained by the fact the loading pressure of ~ 100 bar was not known precisely.

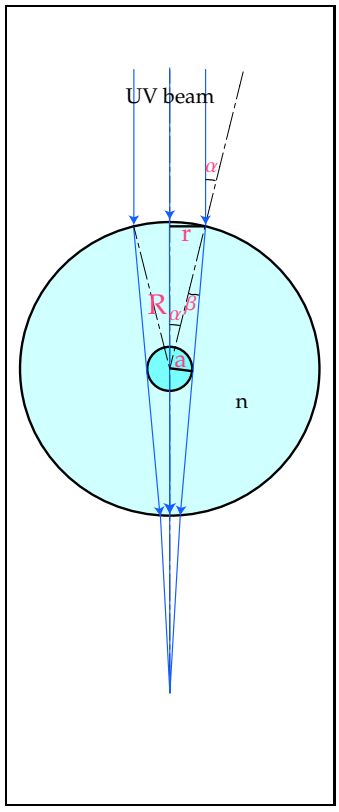

A useful generalization of the model could be to choose the unknown parameters in such a way that the model also describes other type of optical waveguides, not only optical fibers that the parameters have been optimized for. As one can see in the figure to the left, an optical fiber works as an optical lens for the UV light. Simple geometrical calculations below show that a fiber's core with refractive index n of the cladding effectively gets n times as much UV light as a planar waveguide would get under the same exposure conditions.

$$\begin{cases} \sin\alpha = r/R, \\ \sin\beta = (\sin\alpha)/n = r/(nR), \\ a/R = \sin\beta = r/(nR), \\ r = n\,a. \end{cases}$$

In the calculations above, a is radius of the fiber's core, n is the refractive index of its cladding at wavelength of the illuminating UV light, R is the cladding's radius. The meaning of the geometrical parameters α, β and r is clear from the picture.

Thus the last equation

$$\boxed{\frac{r}{a} = n}$$

shows that an optical fiber functions as an optical lens delivering $n \approx 1.5$ as

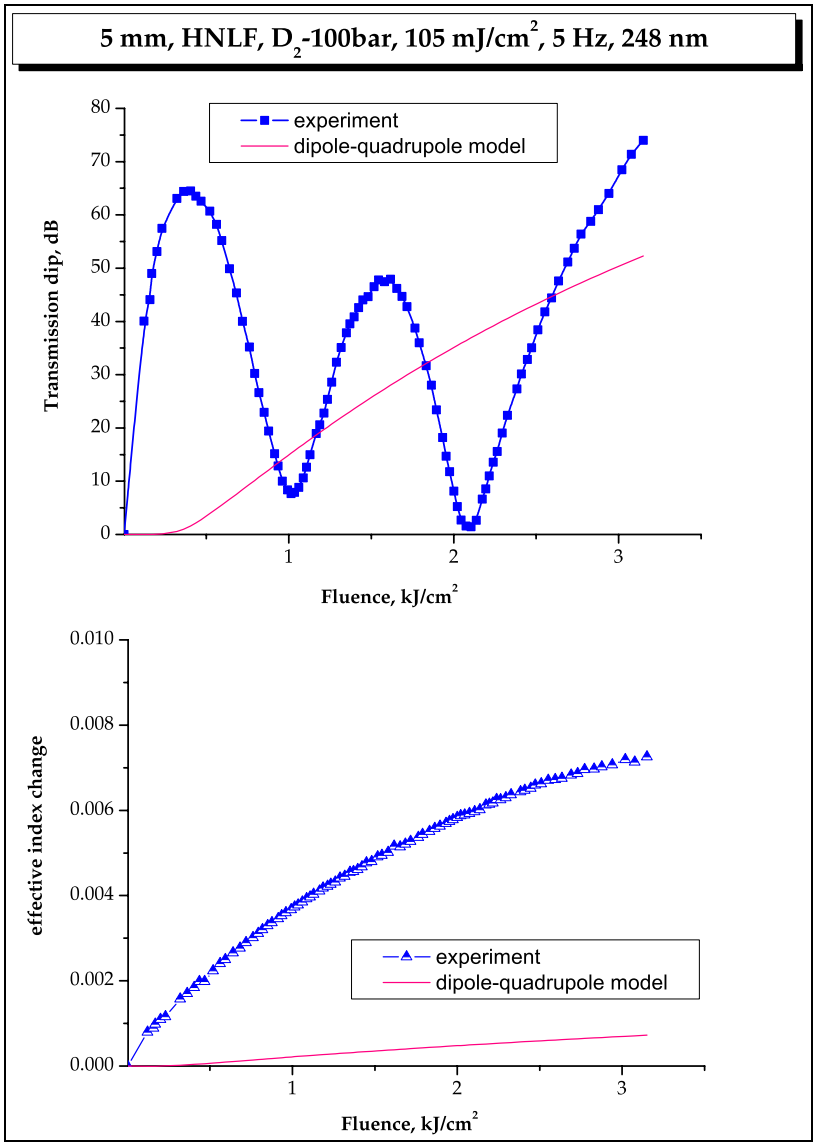

Figure 2.2: *Comparison between experimental results and predictions of the dipole-quadrupole theory for a 5 mm long uniform grating written in deuterium loaded HNLF fiber. UV laser parameters: 248 nm excimer pulse laser at 5 Hz and 105 mJ/cm^2 pulse fluence.*

much UV radiation to the fiber's core as a planar waveguide would do. If one takes this into account by multiplying the power delivered to core by n and adjusts the model's unknown parameters using the new value of UV intensity in the fiber's core, then the model should be able to describe all kinds of optical waveguides, not only fibers. There is of course a question about reflection at the core-cladding border but it should not be of any significance because of a small difference in the refractive indices of the core and the cladding of the fiber.

Chapter 3

Fiber Bragg grating theory

In this chapter the main features of the mathematical model for fiber Bragg gratings will be derived. Most of the results of this chapter are well-known and have been published in the literature [3, 4, 39]. Nevertheless there are several reasons that make it appropriate to reproduce the most important aspects of the theory here:

- this chapter will make the thesis more complete for those readers who are interested in theoretical questions and will reduce their need to search for other sources of information,
- it will concentrate on the application of the fiber Bragg grating theory to the issues dealt with in the thesis such as *polarization control method* (section 4.1) and grating design using *Levenberg-Marquardt method* (section 5.1),
- it will be hopefully useful for my colleges who will continue working on fiber Bragg grating design and fabrication, and who will use this thesis as a reference book.

The derivation given in the chapter and throughout the thesis describe *single-mode fibers* and they cover such topics as *fiber optics*, *coupled mode theory* and *transfer matrix method*.

3.1 Fiber optics

As mentioned in section 1.1, one has to solve the general *Maxwell's equations* in order to describe propagation of the infra-red light through optical fibers. This is explained by the fact the wavelengths of the propagating light are compared to the diameter of the fiber's core.

3.1.1 Maxwell's equations

We determine the electric and magnetic fields of guided waves that satisfy *Maxwell's equations* and the boundary conditions imposed by the cylindric dielectric core and cladding. We will show that there are certain solutions, called *modes*, each with its own *propagation constant* and field distribution in the transverse plane. Only *single mode fibers* will be dealt with in this thesis, both for the sake of simplicity and because of the fact that only this kind of fibers has been used in the experimental part of thesis. The *Maxwell's equations* that describe the electromagnetic field state [40]:

$$\boxed{\begin{aligned} \nabla \times \mathbf{E} &= -\frac{\partial \mathbf{B}}{\partial t}, \\ \nabla \times \mathbf{H} &= \frac{\partial \mathbf{D}}{\partial t} + \mathbf{J}, \\ \nabla \cdot \mathbf{D} &= \rho, \\ \nabla \cdot \mathbf{B} &= 0, \end{aligned}} \tag{3.1-1}$$

where $\mathbf{E}$ and $\mathbf{H}$ are *electric* and *magnetic field* vectors respectively, $\mathbf{B}$ and $\mathbf{D}$ are *magnetic flux* and *magnetic displacement* vectors, while $\mathbf{J}$ and ρ are *displacement current* and *volume charge density* respectively. The latter two are equal to 0 in the dielectric media of the fiber with no free charges:

$$\begin{cases} \mathbf{J} = 0, \\ \rho = 0. \end{cases} \tag{3.1-2}$$

The *Maxwell's equations* (3.1-1) should be combined with the *constitutive relations* that characterizes given media where the electromagnetic waves are propagating:

$$\begin{cases} \mathbf{D} = \epsilon_0 \mathbf{E} + \mathbf{P}, \\ \mathbf{B} = \mu_0 \mathbf{H}, \end{cases} \tag{3.1-3}$$

where $\mathbf{P}$ is *induced polarization*, ϵ_0 is the *dielectric constant* and μ_0 is the *magnetic permeability*.

The dielectric media of the fiber can be considered to be linear for the those weak intensities of the infrared light that propagates through the fiber i.e. $\mathbf{P} = \epsilon_0 \chi \mathbf{E}$, where χ the *linear susceptibility* of the media. This leads to the proportionality between $\mathbf{D}$ and $\mathbf{E}$:

$$\mathbf{D} = \epsilon_0 \epsilon \mathbf{E}, \tag{3.1-4}$$

where $\epsilon = 1 + \chi$ is *relative permittivity* of the media which is connected to the refractive index n by

$$\epsilon = n^2. \tag{3.1-5}$$

3.1.2 Wave equation

Using equations (3.1-1), (3.1-2), (3.1-3) and (3.1-4) we can obtain a so-called *wave equation* for vector $\mathbf{E}$ if we define following complex notation for the electric field $\mathbf{E}$ that represents a Fourier component of the field with *angular frequency* ω and *propagation constant* β and complex amplitude $\vec{E}$:

$$\mathbf{E} = \mathfrak{Re}\left[\vec{E}\, e^{i(\beta z - \omega t)}\right], \tag{3.1-6}$$

where $\mathfrak{Re}(z)$ stands for a real part of a complex number z. In the above equation z is a coordinate in the direction of wave propagation.

The electric field in the fiber is described by the *wave equation* written using the cylindrical coordinates ρ, ϕ and z:

$$\left[\nabla^2 + \left(\frac{\omega}{c}\right)^2 n^2(\rho, \phi, z)\right] \vec{E}(\rho, \phi, z) = 0, \tag{3.1-7}$$

where $c = 1/\sqrt{\epsilon_o \mu_o}$ is the *speed of light* in vacuum. From equations (3.1-6) and (3.1-7) one can easily see that the field components can be separated from each other $\left|\vec{E}(\rho, \phi, z)\right| = E_{\|}(z)\,\Psi(\rho, \phi)$:

$$\frac{d^2 E_{\|}(z)}{dz^2} + \beta^2 E_{\|}(z) = 0, \tag{3.1-8}$$

and

$$\left[\nabla_{\perp}^2 + \left(\frac{\omega}{c}\right)^2 n^2(\rho) - \beta^2\right] \Psi(\rho, \phi) = 0, \tag{3.1-9}$$

where transverse component of the electric field $\Psi(\rho, \phi)$ does not depend on ϕ in the case of a single mode fiber. The transverse component of the *Laplacian* $\nabla_{\perp}^2$ is given by:

$$\nabla_{\perp}^2 = \frac{1}{\rho}\frac{\partial}{\partial \rho}\left(\rho \frac{\partial}{\partial \rho}\right) + \frac{1}{\rho^2}\frac{\partial^2}{\partial \phi^2}.$$

If a is the fiber core's radius then the refractive index n is given by the following equation as shown in Fig. 1.1:

$$n(\rho, \phi, z) = n(\rho) = \begin{cases} n_{\text{core}} & \text{for } \rho \leqslant a, \\ n_{\text{clad}} & \text{for } \rho > a. \end{cases} \tag{3.1-10}$$

In this case the wave equation (3.1-9) can be solved analytically assuming that the fiber radius is much larger than its core radius [41]. The general solution

is expressed by *Bessel functions* $J_m(x)$ and $K_m(x)$ for $m = 0, 1, 2, 3\ldots$ For the transverse component of the electrical field one can write

$$\Psi(\rho, \phi) = \begin{cases} A\, J_m(x\rho) \exp(im\phi) \exp(i\beta z) & \text{for } \rho \leqslant a, \\ C\, K_m(\gamma\rho) \exp(im\phi) \exp(i\beta z) & \text{for } \rho > a, \end{cases} \tag{3.1-11}$$

where A and C are some normalization constants and

$$\begin{aligned} x^2 &= (\omega/c)^2\, n_{\text{core}}^2 - \beta^2, \\ \gamma^2 &= \beta^2 - (\omega/c)^2\, n_{\text{clad}}^2. \end{aligned} \tag{3.1-12}$$

One can readily see that

$$x^2 + \gamma^2 = \left(n_{\text{core}}^2 - n_{\text{clad}}^2\right)(\omega/c)^2\,. \tag{3.1-13}$$

For a *single-mode fiber* equation (3.1-11) can be simplified as we have $m = 0$ in this case. Furthermore, requiring a continuity of E_z at the core-cladding boundary for $\rho = a$ in equation (3.1-10) we get the following dependency for $\Psi(\rho)$ as a function of radial distance ρ:

$$\Psi(\rho) \propto \begin{cases} J_0(x\rho)/J_0(xa) & \text{for } \rho \leqslant a, \\ K_0(\gamma\rho)/K_0(\gamma a) & \text{for } \rho > a. \end{cases} \tag{3.1-14}$$

3.1.3 Effective refractive index

Most fibers are *weakly guiding*, i.e. $n_{\text{core}} \approx n_{\text{clad}}$ [13]. One can show that for weakly guiding fibers the derivative of the field (3.1-14) must be continuous on the core-cladding boundary as well. This imposes an additional equation for $X \equiv xa$ and $Y \equiv \gamma a$:

$$X \frac{J_1(X)}{J_0(X)} = Y \frac{K_1(Y)}{K_0(Y)}. \tag{3.1-15}$$

One can rewrite equation (3.1-13) as

$$X^2 + Y^2 = V^2, \tag{3.1-16}$$

where $V = (\omega\, a/c)\left(n_{\text{core}}^2 - n_{\text{clad}}^2\right)^{1/2}$ is *normalized frequency*. It can be shown [41, 42] that a step-index fiber has only one propagating mode if

$$V < \alpha \approx 2.405, \tag{3.1-17}$$

where α is the first positive root of the equation $J_0(\alpha) = 0$.

Equations (3.1-15) together with (3.1-16) determine X and Y and hereby x, γ and β. The effective refractive index $n_{\text{eff}}(\omega)$ of the propagating electromagnetic wave is defined as

$$\boxed{n_{\text{eff}}(\omega) = \beta(\omega)\, c/\omega.} \tag{3.1-18}$$

3.1.4 Confinement factor

Confinement factor Γ is the fraction of modal power that is contained in the core where the UV photosensitive refractive index change occurs. In cylindrical coordinates of the optical fiber it takes the following form:

$$\Gamma = \frac{\int_0^a |\Psi(\rho)|^2 \rho \, d\rho}{\int_0^\infty |\Psi(\rho)|^2 \rho \, d\rho}, \tag{3.1-19}$$

where $\Psi(\rho)$ is given by equation (3.1-14). The integral (3.1-19) can be readily calculated analytically if the following integrals are used [43]:

$$\int_0^X t J_0^2(t)\, dt = \frac{X^2}{2}\left[J_0^2(X) + J_1^2(X)\right] \quad \text{and} \quad \int_Y^\infty t K_0^2(t)\, dt = \frac{Y^2}{2}\left[K_1^2(Y) - K_0^2(Y)\right].$$

Thus we have:

$$\boxed{\Gamma = K_0^2(Y)\,\frac{J_0^2(X) + J_1^2(X)}{J_0^2(X)\,K_1^2(Y) + J_1^2(X)\,K_0^2(Y)},} \tag{3.1-20}$$

where X and Y are defined by $X \equiv xa$ and $Y \equiv \gamma a$ as above.

When exposed to UV radiation, the refractive index of a photosensitive fiber core changes its value. This leads to the change of the effective refractive index. Due to the small changes $\Delta n_{\text{eff}} \ll n_{\text{eff}}$ and $\Delta n_{\text{core}} \ll n_{\text{core}}$, one can assume a direct proportionality between Δn_{eff} and Δn_{core}. The proportionality coefficient can be easily found using definition of the effective refractive index (3.1-18) and (3.1-12). Simple but slightly cumbersome calculations lead to the following result:

$$\frac{dn_{\text{eff}}}{dn_{\text{core}}} = \frac{n_{\text{core}}}{n_{\text{eff}}}\,K_0^2(Y)\,\frac{J_0^2(X) + J_1^2(X)}{J_0^2(X)\,K_1^2(Y) + J_1^2(X)\,K_0^2(Y)}.$$

Comparing this result to equation (3.1-20) we have:

$$\frac{dn_{\text{eff}}}{dn_{\text{core}}} = \Gamma\,\frac{n_{\text{core}}}{n_{\text{eff}}} \approx \Gamma,$$

so that we have the following relation between Δn_{eff} and Δn_{core} which is a good approximation for a majority of practical situations:

$$\boxed{\Delta n_{\text{eff}} \approx \Gamma \Delta n_{\text{core}}.} \tag{3.1-21}$$

Since the change in the effective refractive index is a consequence of the change in the refractive index of the fibers core, it is more practical to rewrite equations as (1.2-3)

$$\begin{cases} \sigma(z) = \Gamma\, n_{\text{ave}}(z) \big/ n_0, \\ \kappa(z) = \Gamma\, n_{\text{mod}}(z) \big/ n_0, \end{cases} \tag{3.1-22}$$

where $n_{\text{ave}}(z)$ is the average refractive index change in the core of the fiber, n_{mod} is the amplitude of the core's refractive index change and as before n_0 is the unperturbed effective refractive index of the fiber without the Bragg grating.

3.2 Coupled-mode theory

Coupled-mode theory is an intuitive and straightforward model that accurately describes fiber Bragg gratings. It is discussed in details in a large number of articles and books [4, 41, 44–49]. The grating is treated as a perturbation to the fiber. This means that $\sigma(\zeta)$ and $\kappa(\zeta)$ in equation (1.3-8) must be much smaller than one for all ζ. In the presence of a Bragg grating equation (3.1-8) looks like:

$$\frac{d^2 E_{\parallel}(z)}{dz^2} + k^2 \left[\frac{n_{\text{eff}}(z)}{n_0} \right]^2 E_{\parallel}(z) = 0, \tag{3.2-1}$$

where n_0 is effective refractive index of the unperturbed fiber without the grating, $k = \omega n_0 / c$ and $n_{\text{eff}}(z)/n_0$ is given by (1.3-7). The wave number k_0 from equation (1.3-4) identifies the *nominal wave number* of light at the Bragg scattering resonance (1.3-5), and the corresponding *nominal resonance frequency* $\omega_0 \equiv c\, k_0 / n_0$.

It is convenient to define a *detuning parameter* in order to proceed further:

$$\boxed{\delta \equiv \frac{\omega - \omega_0}{\omega_0}.} \tag{3.2-2}$$

Using this definition we can rewrite equation (3.2-1) in terms of $\zeta \equiv k_0 z$ as an independent dimensionless variable

$$\frac{d^2 E_{\parallel}(\zeta)}{d\zeta^2} + \left\{ 1 + 2\left[\sigma(\zeta) + \delta\right] + 2\kappa(\zeta)\exp(+i\gamma) + 2\kappa(\zeta)\exp(-i\gamma) \right\} E_{\parallel}(\zeta) = 0, \tag{3.2-3}$$

where $\gamma \equiv 2\zeta + \varphi(\zeta)$.

In the absence of the grating ($\sigma, \kappa = 0$) the solution to the above equation in the vicinity of $\delta = 0$ looks like

$$E_{\parallel}(\zeta) = a_+ \exp(+i\zeta) + a_- \exp(-i\zeta).$$

Therefore as a first order approximation one chooses to look for a solution to equation (3.2-3) in the form:

$$E_{\parallel}(\zeta) \equiv E_{\parallel}^{+}(\zeta) + E_{\parallel}^{-}(\zeta) = a_{+}(\zeta)\exp(i\zeta) + a_{-}(\zeta)\exp(-i\zeta)\,. \tag{3.2-4}$$

The two terms in this equation describe the forward and backwards propagating modes respectively. It is convenient to write $a_{+}(\zeta)$ and $a_{-}(\zeta)$ as

$$\begin{cases} a_{+}(\zeta) = u(\zeta)\exp\left[+\dfrac{i}{2}\varphi(\zeta)\right], \\ \\ a_{-}(\zeta) = v(\zeta)\exp\left[-\dfrac{i}{2}\varphi(\zeta)\right], \end{cases} \tag{3.2-5}$$

so that we have

$$\begin{cases} E_{\parallel}^{+}(\zeta) = u(\zeta)\exp\left[+i\gamma(\zeta)/2\right], \\ E_{\parallel}^{-}(\zeta) = v(\zeta)\exp\left[-i\gamma(\zeta)/2\right]. \end{cases} \tag{3.2-6}$$

Using (3.2-6) one can rewrite equation (3.2-4) as

$$E_{\parallel}(\zeta) = u(\zeta)\exp\left[+\frac{i\gamma(\zeta)}{2}\right] + v(\zeta)\exp\left[-\frac{i\gamma(\zeta)}{2}\right]. \tag{3.2-7}$$

Inserting equation (3.2-7) into (3.2-3), ignoring the terms that are rapidly oscillating and collecting together the terms with $\exp\left[i\gamma(\zeta)/2\right]$ and $\exp\left[-i\gamma(\zeta)/2\right]$, we get the *coupled-mode equations* that describe the coupling between the two counter-propagating modes [46]:

$$\boxed{\begin{aligned} \frac{du(\zeta)}{d\zeta} &= +i\left[\hat{\sigma}(\zeta)u(\zeta) + \kappa(\zeta)v(\zeta)\right], \\ \\ \frac{dv(\zeta)}{d\zeta} &= -i\left[\hat{\sigma}(\zeta)v(\zeta) + \kappa(\zeta)u(\zeta)\right], \end{aligned}} \tag{3.2-8}$$

where

$$\hat{\sigma}(\zeta) = \sigma(\zeta) + \delta - \frac{1}{2}\frac{d\varphi(\zeta)}{d\zeta}\,. \tag{3.2-9}$$

These equations (3.2-8) describe coupling, i.e. energy exchange between the two counter-propagating modes. Multiplying the first of these equations by $u^{*}(\zeta)$ and the second one by $v^{*}(\zeta)$ we get:

$$u^{*}(\zeta)\frac{du(\zeta)}{d\zeta} - v^{*}(\zeta)\frac{dv(\zeta)}{d\zeta} = i\left\{\hat{\sigma}(\zeta)\left[|u(\zeta)|^2 + |v(\zeta)|^2\right] + \kappa(\zeta)\left[v(\zeta)u^{*}(\zeta) + u(\zeta)v^{*}(\zeta)\right]\right\}.$$

Using the fact that $\sigma(\zeta)$ and $\kappa(\zeta)$ are real functions, we can add the last equation with its complex conjugate to get an equation which expresses *energy conservation* between the two modes (despite of energy exchange between them):

$$\boxed{\frac{d}{d\zeta}\left[|u(\zeta)|^2 - |v(\zeta)|^2\right] = 0.} \tag{3.2-10}$$

In order to solve the *coupled-mode equations* (3.2-8) one has to impose some *boundary conditions*. This is done by the physical interpretation of the coupled modes. The amplitude of the backward propagating mode, given by $v(\zeta)$ should be equal to zero for all possible δ at $\zeta = \zeta_L \equiv k_0 L$, where the grating ends. (Here we assume that the grating has length L and that it spans from $\zeta = 0$ to $\zeta = \zeta_L$). We have a system of *boundary conditions* that have to be solved together with the *coupled-mode equations* (3.2-8) and (3.2-9):

$$\boxed{\begin{array}{l} u(0;\delta) = u_0, \\ v(\zeta_L;\delta) = 0. \end{array}} \tag{3.2-11}$$

One can define the *reflection coefficient* $r(\delta)$ and the *transmission coefficient* $t(\delta)$ of the grating in terms of u and v in the following way:

$$\boxed{\begin{array}{l} r(\delta) = a_-(0)/a_+(0) = e^{-i\varphi_0}\, v(0)/u_0, \\ t(\delta) = a_+(\zeta_L)/a_+(0) = e^{i\varphi(\zeta_L)/2} e^{-i\varphi_0/2}\, u(\zeta_L)/u_0, \end{array}} \tag{3.2-12}$$

where $\varphi_0 \equiv \varphi(0)$.

3.3 Weak gratings

Weak Bragg gratings are the gratings with small *coupling coefficient* $\kappa \to 0$. In this case we can use the first-order *Born approximation* [50]. This approximation means that the forward propagating wave is unaffected by the grating, i.e.

$$u(\zeta) = u_0 \exp\left[i \int_0^\zeta \hat{\sigma}(t) dt \right],$$

which is obtained from the *boundary condition* (3.2-11) and the *coupled-mode equations* (3.2-8) when $\kappa(\zeta) = 0$. This expression for $u(\zeta)$ should be substituted into the second equation in (3.2-8), and the resulting first-order equation for $v(\zeta)$ should be solved with the *boundary conditions* $v(\infty;\delta) = 0$ and $v(0,\delta) = r(\delta)\, u_0\, e^{i\varphi_0}$. The result is

$$v(\zeta;\delta) = -u_0 \exp\left[-i \int_0^\zeta \hat{\sigma}(t)\, dt \right] \int_\zeta^\infty Q^*(\zeta')\, d\zeta'$$

and

$$r(\delta) = e^{-i\varphi_0}\, v(0;\delta)\big/ u_0 = -\int_0^\infty Q^*(\zeta)\, d\zeta, \tag{3.3-1}$$

where

$$Q(\zeta) \equiv i\kappa(\zeta)\, e^{i\varphi_0} \exp\left[-2i\int_0^\zeta \hat{\sigma}(t)\, dt\right].$$

Using the definition of $\hat{\sigma}(\zeta)$ (3.2-9) we can rewrite the last equation (3.3-1) in the following way:

$$r(\delta) = -\int_0^\infty q^*(\zeta)\, \exp(2i\,\delta\,\zeta)\, d\zeta \tag{3.3-2}$$

or

$$\boxed{r(\delta) = -\frac{1}{2}\int_0^\infty q^*\left(\frac{\zeta}{2}\right) \exp(i\,\delta\,\zeta)\, d\zeta.} \tag{3.3-3}$$

We can see that $r(\delta)$ does not depend on u_0 as expected. In the last equation (3.3-3)

$$\boxed{q(\zeta) \equiv i\,\kappa(\zeta) \exp\left[i\varphi(\zeta) - 2i\int_0^\zeta \sigma(t)\, dt\right]} \tag{3.3-4}$$

is a *complex coupling coefficient*.

Thus, in the first order *Born approximation* the reflection coefficient $r(\delta)$ is given by the *Fourier transform* of the *complex coupling coefficient*. If we have a *uniform grating* $\sigma(\zeta) \equiv \sigma$, $\kappa(\zeta) \equiv \kappa$ and $\varphi(\zeta) \equiv \varphi_0$, then from (3.3-4)

$$q^*(\zeta) = -i\,\kappa\, e^{-i\varphi_0} \exp(2i\,\sigma\zeta).$$

This gives rise to the reflection coefficient $r(\delta)$ of the grating with normalized length ζ_L :

$$r(\delta) = i\,\kappa\,\zeta_L\, \mathrm{sinc}\left(\hat{\sigma}\zeta_L\right) e^{i\varphi_0}\, e^{i\hat{\sigma}\zeta_L}, \tag{3.3-5}$$

where $\hat{\sigma} = \sigma + \delta$ according to (3.2-9) and $\mathrm{sinc}\, x \equiv (\sin x)/x$.

3.4 Uniform fiber Bragg grating

Uniform fiber Bragg grating is characterized by constant values of $\sigma(\zeta) \equiv \sigma$, $\kappa(\zeta) \equiv \kappa$ and $\varphi(\zeta) \equiv \varphi_0$. In this case the *coupled-mode equations* (3.2-8)

can be solved analytically. By differentiating the *coupled-mode equations* and substituting them again in stead of the first-order derivatives, we get:

$$\begin{cases} \dfrac{d^2u(\zeta)}{d\zeta^2} = \xi^2 u(\zeta), \\ \dfrac{d^2v(\zeta)}{d\zeta^2} = \xi^2 v(\zeta), \end{cases} \tag{3.4-1}$$

where

$$\xi \equiv \left(\kappa^2 - \hat{\sigma}^2\right)^{1/2}.$$

This shows that the *band gap* of a uniform grating is given by $|\hat{\sigma}| \leqslant \kappa$ or according to (3.2-9)

$$|\delta + \sigma| \leqslant \kappa. \tag{3.4-2}$$

Equations (3.4-1) should be solved using the *boundary conditions* (3.2-11). Knowing $u(\zeta)$ and $v(\zeta)$, we can find transmission t and reflection r using their definition (3.2-12). The result is [51, 52]:

$$\begin{aligned} t(\delta) &= \left[\cosh\left(\xi\zeta_L\right) - \frac{i\hat{\sigma}}{\xi}\sinh\left(\xi\zeta_L\right)\right]^{-1}, \\ r(\delta) &= \left(i\kappa/\xi\right)e^{i\varphi_0}\sinh\left(\xi\zeta_L\right)\left[\cosh\left(\xi\zeta_L\right) - \frac{i\hat{\sigma}}{\xi}\sinh\left(\xi\zeta_L\right)\right]^{-1}. \end{aligned} \tag{3.4-3}$$

If we now consider a *weak uniform grating* for which $\xi \approx i\hat{\sigma}$, then we get an expression for $r(\delta)$ which coincides with equation (3.3-5) as expected.

3.5 Spectral characteristics of Bragg gratings

Using boundary conditions (3.2-11) one can define such properties of a grating as its *reflection* $r(\omega)$ and *transmission* $t(\omega)$ (3.2-12) as well as its *reflectivity* and its *transmittivity*

$$\boxed{\begin{array}{l} R(\omega) \equiv |r(\omega)|^2, \\ T(\omega) \equiv |t(\omega)|^2. \end{array}} \tag{3.5-1}$$

Spectral properties of a grating can be measured from two different sides (from its front and from its back). One can show that these two type of measurement give the same result for transmission $t(\omega)$ and in general different results for reflection $r(\omega)$ which we will denote $r^+(\omega)$ and $r^-(\omega)$. They have

the same amplitude or *reflectivity* $R(\omega)$ but different phases [44,53]. In general the following two equations are valid for a *lossless grating* [53,54]:

$$\begin{cases} \left|r^{\pm}\right|^2 + |t|^2 = 1, \\ r^{+}\big/(r^{-})^{*} = -t/t^{*}. \end{cases} \tag{3.5-2}$$

Dispersion properties of a grating are often given by its *group delay* in transmission $D_t(\omega)$ defined in terms of the *accumulative phase* ϕ_t of the transmission coefficient $t(\omega)$ by the equation $D_t(\omega) = \partial\phi_t(\omega)/\partial\omega$ and the two *group delays* in reflection $D_r^{\pm}(\omega) = \partial\phi_r^{\pm}(\omega)/\partial\omega$ defined in terms of the *accumulative phases* of $r^{\pm}(\omega)$ respectively. These five quantities are related to each other by simple equations that follow from (3.5-2):

$$R(\omega) + T(\omega) = 1, \tag{3.5-3}$$

$$D_r^{+}(\omega) + D_r^{-}(\omega) = 2D_t(\omega). \tag{3.5-4}$$

Moreover, the group delay $D_t(\omega)$ in transmission and the transmissivity $T(\omega)$ are related by the following equation given in the form of a *Hilbert transform*:

$$D_t(\omega) - D_0 = -\frac{1}{\pi} \fint_{-\infty}^{\infty} \frac{\partial \log\sqrt{T(\omega')}}{\partial\omega'} \frac{\mathrm{d}\omega'}{\omega' - \omega}, \tag{3.5-5}$$

where $\fint$ denotes the principal value of the integral and the constant $D_0 \equiv D_t(\infty)$ is equal to the propagation delay in the absence of the grating [53]. Equation (3.5-5) is a consequence of the fact that the transmission coefficient $t(\omega)$ and its reciprocal $1/t(\omega)$ are *causal functions* (i.e. their Fourier transforms are equal to zero for negative times) [45]. In general, a grating exists that corresponds to any causal reflection coefficients $r(\omega)$. This is not true for any causal transmission coefficient $t(\omega)$ because its real and imaginary parts have to be related to each other by equation (3.5-5).

Finally, *dispersion* $d(\omega)$ is defined as a derivative of the *group delay* with respect to the wavelength $\lambda = 2\pi c/\omega$:

$$d_x(\omega) = \frac{dD_x(\lambda)}{d\lambda} = \left(\frac{dD_x(\omega)}{d\omega}\right)\Big/\left(\frac{d\lambda}{d\omega}\right) = -\frac{2\pi c}{\omega^2}\frac{dD_x(\omega)}{d\omega}, \tag{3.5-6}$$

where x stands for three different types of *dispersion* t, r^{+} and r^{-}, i.e. dispersion in transmission d_t and two dispersions in reflection $d_r^{\pm}$.

It should be noticed that $r^{-}(\omega) = r^{+}(\omega)$ in a case of a *symmetric grating* [53]. In this have we have the following relations as well

$$D_t(\omega) = D_r^{+}(\omega) = D_r^{-}(\omega)$$

and

$$d_t(\omega) = d_r^{+}(\omega) = d_r^{-}(\omega).$$

3.6 Transfer matrix method

The *transfer matrix method* is based on the fact that it is possible to relate the amplitudes of the forward and backwards propagating waves $u(\zeta + \Delta\zeta)$ and $v(\zeta + \Delta\zeta)$ at the position $\zeta + \Delta\zeta$ along the grating with their values $u(\zeta)$ and $v(\zeta)$ at ζ, if we know the spectral characteristics of the that part of the waveguide that lies between ζ and $\zeta + \Delta\zeta$.

We can write [39,55]:

$$\begin{bmatrix} u(\zeta) \\ v(\zeta) \end{bmatrix} = \hat{\mathbf{T}} \begin{bmatrix} u(\zeta + \Delta\zeta) \\ v(\zeta + \Delta\zeta) \end{bmatrix}, \tag{3.6-1}$$

where

$$\hat{\mathbf{T}} \equiv \begin{bmatrix} \hat{\mathbf{T}}_{1,1} & \hat{\mathbf{T}}_{1,2} \\ \hat{\mathbf{T}}_{2,1} & \hat{\mathbf{T}}_{2,2} \end{bmatrix} = \begin{bmatrix} t - r^+ r^- / t & r^- / t \\ -r^+ / t & 1/t \end{bmatrix}. \tag{3.6-2}$$

For a *lossless grating* we can rewrite (3.6-2) using equation (3.5-2):

$$\hat{\mathbf{T}} = \begin{bmatrix} 1/t^* & r^- / t \\ -r^+ / t & 1/t \end{bmatrix} = \begin{bmatrix} 1/t^* & -(r^+ / t)^* \\ -r^+ / t & 1/t \end{bmatrix}. \tag{3.6-3}$$

It should be noticed that for a *lossless grating* equation (3.6-3) leads to

$$\boxed{\det(\hat{\mathbf{T}}) = 1,}$$

which expresses the *energy conservation*.

If the grating is divided into a large number N of parts, then we can consider each part of the grating to be uniform with reflection $r(\delta)$ and transmission $t(\delta)$ given by equations (3.4-3). The part of the grating with number i is situated at $\zeta \equiv \zeta_i$, has normalized length $\Delta\zeta_i$ and coupling coefficient $\kappa_i \equiv \kappa(\zeta_i)$ and $\hat{\sigma}_i \equiv \hat{\sigma}(\zeta_i)$. The *transform matrix* $\hat{\mathbf{T}}_i$ of this part is given by the following equation according to (3.6-3) and (3.4-3):

$$\hat{\mathbf{T}}_i = \begin{bmatrix} \cosh(\xi_i \Delta\zeta_i) + \dfrac{i\hat{\sigma}_i}{\xi_i} \sinh(\xi_i \Delta\zeta_i) & (i\kappa_i / \xi_i) e^{i\varphi_i} \sinh(\xi_i \Delta\zeta_i) \\ -(i\kappa_i / \xi_i) e^{-i\varphi_i} \sinh(\xi_i \Delta\zeta_i) & \cosh(\xi_i \Delta\zeta_i) - \dfrac{i\hat{\sigma}_i}{\xi_i} \sinh(\xi_i \Delta\zeta_i) \end{bmatrix}, \tag{3.6-4}$$

where $\xi_i \equiv (\kappa_i^2 - \hat{\sigma}_i^2)^{1/2}$ and $\varphi_i \equiv \varphi(\zeta_i)$.

Thus, dividing a *non-uniform grating* into a large number N of *uniform gratings*, we can find a *transfer matrix* $\hat{\mathbf{T}}$ of the whole grating as

$$\boxed{\hat{\mathbf{T}} = \prod_{i=0}^{N-1} \hat{\mathbf{T}}_{N-i}.} \tag{3.6-5}$$

This gives us an immediate opportunity to find the spectral characteristics $t(\delta)$ and $r^{\pm}(\delta)$ of the whole *non-uniform grating* using equation (3.6-3):

$$\begin{cases} t(\delta) &= 1/\hat{\mathbf{T}}_{2,2}, \\ r^{+}(\delta) &= -\hat{\mathbf{T}}_{2,1}/\hat{\mathbf{T}}_{2,2}, \\ r^{-}(\delta) &= \hat{\mathbf{T}}_{1,2}/\hat{\mathbf{T}}_{2,2}. \end{cases} \tag{3.6-6}$$

Equation (3.6-1) is valid for "transfer" from right to left. It is possible to write it in a way that describes "transfer" from left to right. We can write:

$$\begin{bmatrix} u(\zeta+\Delta\zeta) \\ v(\zeta+\Delta\zeta) \end{bmatrix} = \hat{\mathbf{T}}^{-1} \begin{bmatrix} u(\zeta) \\ v(\zeta) \end{bmatrix}. \tag{3.6-7}$$

Using equation (3.5-2) one can show that

$$\hat{\mathbf{T}}^{-1} = \begin{Vmatrix} 1/t & -r^{-}/t \\ r^{+}/t & 1/t^{*} \end{Vmatrix} = \begin{Vmatrix} 1/t & \left(r^{+}/t\right)^{*} \\ r^{+}/t & 1/t^{*} \end{Vmatrix}. \tag{3.6-8}$$

And the *transfer matrix* $\hat{\mathbf{T}}^{-1}$ of the whole grating is given by an equation similar to equation (3.6-5):

$$\boxed{\hat{\mathbf{T}}^{-1} = \prod_{i=1}^{N} \left(\hat{\mathbf{T}}^{-1}\right)_i}. \tag{3.6-9}$$

It should noted that normally the transfer matrix method uses a special subdivision of the whole grating into uniform parts, namely the parts should all start with the same value of the total phase of the grating. It is however straightforward to generalize the method for arbitrary start phases of different parts. In this case equation (3.6-4) has to be modified. One should use the whole phase of the grating defined in equation (1.2-2) instead of its additional phase $\varphi(z)$. This means that one has to make a substitution in equation (3.6-4)

$$\boxed{\varphi_i \to \frac{2\pi}{\Lambda} z_i + \varphi_i}. \tag{3.6-10}$$

Chapter 4

Bragg grating inscription

Several techniques for controlling the index modulation (or *apodization* profile) during the inscription process have been introduced [8, 56–62] since the side-writing method was discovered by Meltz et al. using coherent UV-light [14]. The simplest approach is to scan an UV-beam over a fixed phase mask/fiber assembly [58]. By post processing the resulting index modulation in a second exposure, apodized gratings can be fabricated [8, 56, 57]. For tailored gratings, a custom made phase mask with the appropriate surface corrugation may be used [59]. Two different sequential writing techniques have been introduced by Stubbe et al. [60] using an *interferometric scanning* technique and by Cole et al. [61] using the *moving fiber/phase mask scanning technique*. These two techniques offer high flexibility for the apodization profile including *multiple phase shifts* and *chirp*, but due to the strict requirements to thermal and vibrational stability, these methods are very expensive and delicate to realize.

In this chapter an alternative flexible and cost-efficient technique is described. It is based on spacial separation of the two polarizations of the incident UV light, and hence its name *Polarization Control Method (PCM)*. It has been developed at the *Bragg grating and poling group*, COM, DTU during the last three years i.e the period of this Ph.D. thesis. We have earlier described the method and the obtained results in a number of articles [63, 64], conference reports [65–72] as well as COM's internal publications [73–77]. A bigger summarizing article is in press at the moment [78].

4.1 Polarization control method – Setup

The experimental setup of the *polarization control method* is schematically illustrated in Fig. 4.1. It is based on controlling the polarization orientation of the UV-beam from a $\lambda_{UV} = 248\,\text{nm}$ KrF *excimer laser* during the process of UV-exposure which is done using a *UV polarizer*. The UV beam is split up into

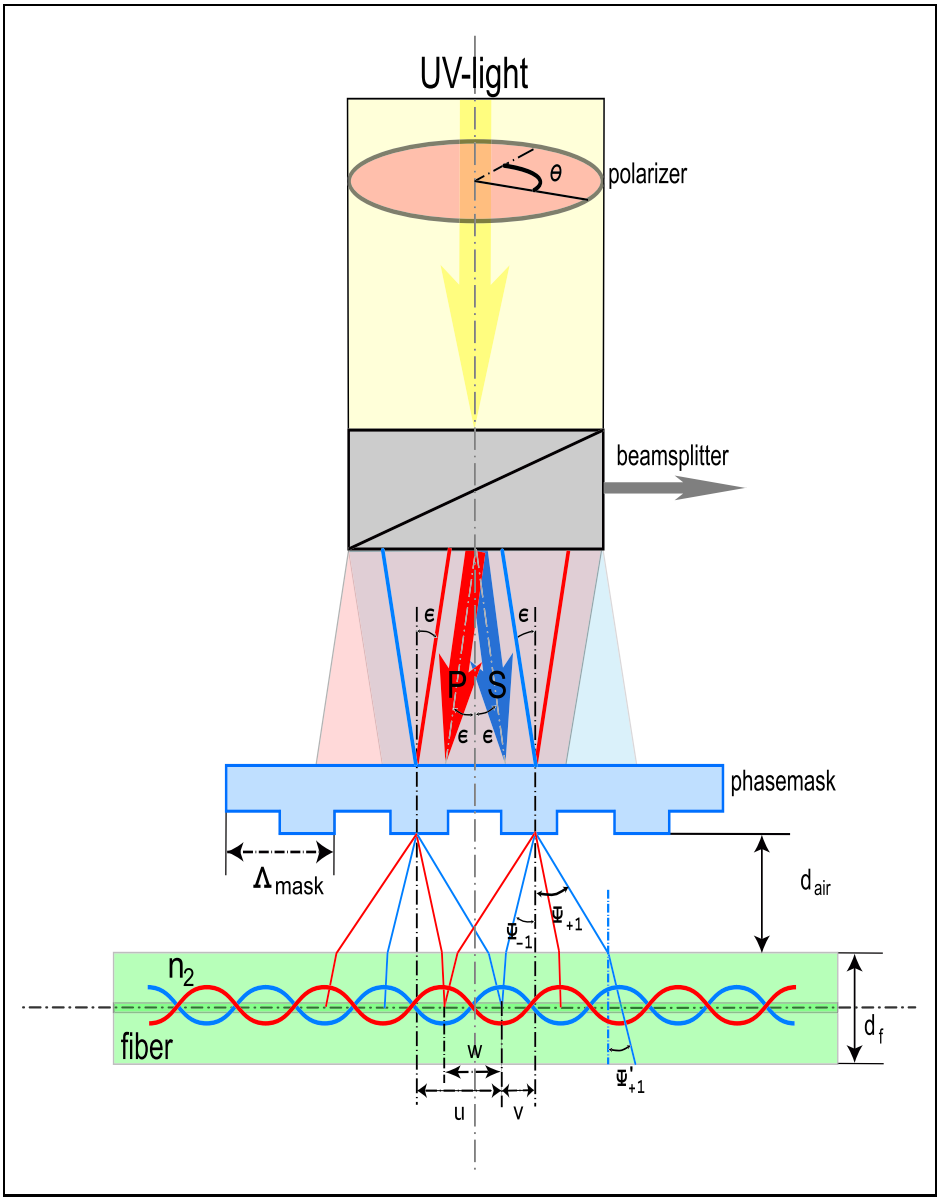

Figure 4.1: *Experimental setup scheme for the polarization control method used at COM; the red and blue colors distinguish between the two different polarizations (s- and p-polarizations) of UV-light that are split by the beamsplitter at the angle 2ϵ to each other.*

two parts with different polarizations (so called *s*- and *p*-polarizations) using a *polarization beamsplitter* that diverges the two polarizations from each other by a small angle $2\epsilon = 0.14^\circ$. The orientation of the polarizer aligned with respect to the fiber and described by angle θ determines the fraction of UV-beam power that is distributed between those two polarizations. According to the *Malus' law* [79] the fraction of energy in those two polarizations are $\mathcal{F}_s$ and $\mathcal{F}_p$ defined by

$$\begin{cases} \mathcal{F}_s = \mathcal{F} \cdot \sin^2\theta, \\ \mathcal{F}_p = \mathcal{F} \cdot \cos^2\theta, \end{cases} \tag{4.1-1}$$

where $\mathcal{F}$ is UV-beam fluence after the polarizer (if we neglect the losses in the beamsplitter). The two different polarizations (red and blue in Fig. 4.1) create two different interference patterns in the fiber as explained below. It is possible to adjust the distance d_{air} between the phase mask and the fiber so that the interference patterns have a phase-shift π between each other, which gives us opportunity to control the amplitude of the resulting interference pattern amplitude A. It is equal to the difference between the two polarizations' fluences as it will be explained below:

$$A = \mathcal{F}_s - \mathcal{F}_p = \mathcal{F} \cdot \left(\cos^2\theta - \sin^2\theta\right) = \mathcal{F} \cdot \cos(2\theta).$$

Thus by controlling the angle θ, one can choose the desired amplitude of the induced Bragg grating at a given position of the laser beam. So by moving the laser beam together with the beamsplitter along the fiber and by controlling the angle θ by a computer program, one can induce a Bragg grating with arbitrary refractive index modulation profile.

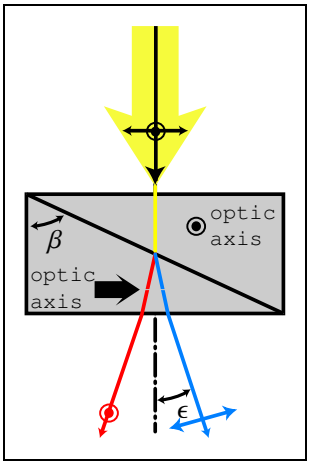

The *polarizing beamsplitter* used in the experiment consists of two air-spaced prisms made of anisotropic (uniaxial) crystals with optic axes directions as shown at the picture to the left. This beamsplitter is referred to as a *Wollaston prism* [13]. When light (polarized or unpolarized) refracts at the surface of an anisotropic crystal the two polarizations refract at different angles and are spatially separated. Those two polarizations are the one which is parallel to the surface between the two prisms and the other one which is perpendicular to it (blue and red color in the picture). The value of the angle ϵ between one of the diverged beams and the original direction of the beam, depends on prism's geometry (its angle β and optic axes orientation) and its refractive indices (there are two of them [80] for any anisotropic uniaxial crystal). In our case we use a beamsplitter which provides an angle $2\epsilon = 0.14^\circ$ between the two polarizations.

4.2 Polarization control method – Theory

Since the *polarization control method* induces a constant average refractive index change n_{ave} along the whole grating (σ = const) and no chirp in the grating $\varphi(\zeta)$ = const, it is convenient to choose another parameter that characterizes the dependency on the light frequency ω. According to equation (3.2-9) one can choose $\hat{\sigma}$ instead of δ. The *central wavelength* λ_c which defines the position of the *transmission peak* of the grating is given by $\hat{\sigma} = 0$ or using equations (3.2-2) and (3.2-9) we can show that

$$\lambda_c = \lambda_0 (1 + \sigma) = \lambda_0 \left(1 + \Gamma \frac{n_{\text{ave}}}{n_0} \right), \tag{4.2-1}$$

where we used equation (3.1-22) and λ_0 is the *Bragg wavelength* of the grating given by (1.2-4) and (1.3-5).

Since gratings fabricated with the *polarization control method* have no *chirp*, i.e. $\sigma(\zeta)$ = const and $\varphi(\zeta)$ = const, their spectra will be symmetric with respect to this central frequency λ_c [53].

4.2.1 Phase mask diffraction

After having passed through the polarizer and the beamsplitter as shown in Fig. 4.1 the UV-light is split into two diverging beams with different polarizations. Depending on the angle θ, the two beams have fluences $\mathcal{F}_s = \mathcal{F} \cdot \cos^2\theta$ and $\mathcal{F}_p = \mathcal{F} \cdot \sin^2\theta$ as mentioned above. The two beam fall at angle $\epsilon = 0.07^\circ$ at the surface of the phase mask. According to equation (1.3-2), both beams will be diffracted by passing through the phase mask with period Λ_{mask}.

The phase mask is produced so that the zero-th order diffraction peak is highly suppressed as described in chapter 3 by equation (1.3-1). The two first order diffraction peaks are characterized by diffraction angles that one can get from (1.3-2) for $m = \pm 1$

$$\sin \Psi^s_{\pm 1} = \pm \frac{\lambda_{\text{UV}}}{\Lambda_{\text{mask}}} + \sin \epsilon, \tag{4.2-2}$$

for *s*-polarization with $\epsilon = 0.07^\circ$ (blue color in Fig. 4.1). The same expression can be written for *p*-polarization except for ϵ should be changed to $-\epsilon$ in equation (4.2-2):

$$\sin \Psi^p_{\pm 1} = \pm \frac{\lambda_{\text{UV}}}{\Lambda_{\text{mask}}} - \sin \epsilon.$$

In our case

$$0.23 \approx \frac{248\,\text{nm}}{1070\,\text{nm}} = \boxed{\frac{\lambda_{\text{UV}}}{\Lambda_{\text{mask}}} \gg \sin \epsilon} = \sin 0.07^\circ \approx 0.00122\,.$$

Here because of the fact that the angle ϵ is very small, one can use the approximation $\sin\epsilon \approx \tan\epsilon \approx \epsilon$, where the angle is measured in radians $\epsilon = 0.07^\circ \approx 0.0122$ radian. By measuring ϵ in radians and by denoting for convenience's sake

$$\tau \equiv \frac{\lambda_{\mathrm{UV}}}{\Lambda_{\mathrm{mask}}},$$

we can write

$$\sin\Psi^{s}_{\pm 1} = \pm\tau + \epsilon \tag{4.2-3}$$

with $\epsilon \ll \tau$ and the corresponding similar expression for $\Psi^{p}_{\pm 1}$.

The angle $\Psi'_{\pm 1}$ is the angle in the fiber's cladding with the refractive index n_2 due the refraction of the beams on the fibers surface. It can be readily found from the *Snell's law* [81] that is valid for both polarizations:

$$\sin\Psi'_{\pm 1} = \frac{\sin\Psi_{\pm 1}}{n_2} = \frac{\pm\tau + \epsilon}{n_2}, \tag{4.2-4}$$

where equation (4.2-3) has been used, n_2 can be taken to be equal to the refractive index of the pure silica at the UV wavelength $\lambda_{\mathrm{UV}} = 248\,\mathrm{nm}$ of the used laser beam. According to [82] $n_2 \approx 1.509$.

Using these expressions for $\Psi_{\pm 1}$ and $\Psi'_{\pm 1}$ we can readily find the distance u in Fig.4.1 expressed through d_{air} (distance between the fiber and the phase mask) and d_{f} (fiber's diameter):

$$u = d_{\mathrm{air}} \cdot \left|\tan\Psi_{+1}\right| + \frac{d_{\mathrm{f}}}{2} \cdot \left|\tan\Psi'_{+1}\right|. \tag{4.2-5}$$

Similar expression can be written for distance v:

$$v = d_{\mathrm{air}} \cdot \left|\tan\Psi_{-1}\right| + \frac{d_{\mathrm{f}}}{2} \cdot \left|\tan\Psi'_{-1}\right|. \tag{4.2-6}$$

So the distance w between the two points where the *s*- and *p*-polarizations converge is equal to:

$$w = u - v = d_{\mathrm{air}} \cdot \left(\left|\tan\Psi_{+1}\right| - \left|\tan\Psi_{-1}\right|\right) + \frac{d_{\mathrm{f}}}{2} \cdot \left(\left|\tan\Psi'_{+1}\right| - \left|\tan\Psi'_{-1}\right|\right), \tag{4.2-7}$$

where we used (4.2-5) and (4.2-6).

4.2.2 Fiber-to-phase-mask distance

Since $\epsilon \ll \tau$, we can use the following approximate expressions that can be derived from equations (4.2-3) and (4.2-4):

$$\begin{cases} \left|\tan\Psi_{+1}\right| - \left|\tan\Psi_{-1}\right| = \dfrac{2\epsilon}{\left(1-\tau^2\right)^{3/2}}, \\ \left|\tan\Psi'_{+1}\right| - \left|\tan\Psi'_{-1}\right| = \dfrac{2\epsilon}{n_2\left(1-\tau^2/n_2^2\right)^{3/2}}. \end{cases} \tag{4.2-8}$$

Remembering that the period of the grating is equal to half of the phase mask's period according to (1.3-3) we get an expression for the spacial phase shift β between the two polarizations if we combine equations (4.2-7) and (4.2-8) together:

$$\beta = 2\pi\frac{w}{\Lambda_{\text{mask}}/2} = \frac{4\pi w}{\Lambda_{\text{mask}}} = \frac{4\pi\epsilon}{\Lambda_{\text{mask}}}\left[\frac{2d_{\text{air}}}{\left(1-\tau^2\right)^{3/2}} + \frac{d_{\text{f}}}{n_2\left(1-\tau^2/n_2^2\right)^{3/2}}\right]. \tag{4.2-9}$$

In the optimal configuration of the experimental setup one has to choose the distance between the fiber and the phase mask so that the phase shift between the two interference patterns is equal to π:

$$\boxed{\beta_{\text{ideal}} = \pi.} \tag{4.2-10}$$

This allows us to find the ideal distance d^*_{air} between the fiber and the phase mask which ensures phase shift π between the two interference patterns:

$$\boxed{d^*_{\text{air}} = \left[\frac{\Lambda_{\text{mask}}}{8\epsilon} - \frac{d_{\text{f}}}{2n_2\left(1-\tau^2/n_2^2\right)^{3/2}}\right]\left(1-\tau^2\right)^{3/2} \approx \frac{\Lambda_{\text{mask}}}{8\epsilon} - \frac{d_{\text{f}}}{2n_2}.} \tag{4.2-11}$$

For the typical values of the parameters in equation (4.2-11) we get an approximate value of the distance d^*_{air}:

$$d^*_{\text{air}} = 68\,\mu\text{m}.$$

Actually, an uncertainty in the technical specifications of the beamsplitter of about $\Delta\epsilon \approx 0.0025^\circ = 5\cdot10^{-5}$ gives rise to an error Δd_{air} in the theoretically calculated value of d_{air}:

$$\left|\Delta d_{\text{air}}\right| = \frac{\Lambda_{\text{mask}}}{8\epsilon^2}\Delta\epsilon = 5\,\mu\text{m}.$$

This gives the final result for the theoretically calculated d^*_{air} :

$$\boxed{d^*_{\text{air}} = (68 \pm 5)\ \mu\text{m}.} \tag{4.2-12}$$

Experimentally found optimal value of d^*_{air} is about $70\,\mu\text{m}$ which agrees perfectly with the theoretically calculated value (4.2-12).

In practical experimental situations, the distance d_{air} can deviate from its ideal value d^*_{air}, giving rise to the deviation $\Delta\beta$ of the phase shift β from its optimal value of π. Equation (4.2-9) leads to the following expression for the phase shift deviation $\Delta\beta$:

$$\Delta\beta = \frac{8\pi\epsilon}{\Lambda_{\text{mask}}\left(1-\tau^2\right)^{3/2}}\,\Delta d_{\text{air}} \approx \frac{8\pi\epsilon}{\Lambda_{\text{mask}}}\,\Delta d_{\text{air}}, \tag{4.2-13}$$

where Δd_{air} is the deviation of d_{air} from its optimal value d_{air} given by equations (4.2-11) and (4.2-12).

4.2.3 Interference pattern

The two interference patterns from the two polarizations of the UV light have the average intensities defined by equation (4.1-1) so that the intensity variations of the UV light along the fiber are given by

$$\begin{cases} \mathcal{F}_p(\zeta) = \mathcal{F}\cdot\cos^2\theta\,[1+\upsilon\cos(2\zeta)], \\ \mathcal{F}_s(\zeta) = \mathcal{F}\cdot\sin^2\theta\,[1+\upsilon\cos(2\zeta+\beta)], \end{cases} \tag{4.2-14}$$

where ζ is a normalized length of the grating defined by equation (1.3-6), υ is the visibility of the interference pattern defined by the UV laser's characteristics [7] and β is the phase shift between the two interference patterns, which is equal to

$$\beta = \pi + \Delta\beta. \tag{4.2-15}$$

The resulting intensity $F(\zeta)$ of the UV light is given by the sum of $\mathcal{F}_s$ and $\mathcal{F}_p$. Using equation (4.2-15), we get

$$F(\zeta) = \mathcal{F}\cos^2\theta + \upsilon\mathcal{F}\cos(2\zeta) + \mathcal{F}\sin^2\theta - \upsilon\mathcal{F}\cos(2\zeta+\Delta\beta), \tag{4.2-16}$$

Since $\cos^2\theta + \sin^2\theta \equiv 1$ and $\cos^2\theta - \sin^2\theta \equiv \cos(2\theta)$, we get in the ideal case when $\Delta\beta = 0$:

$$F(\zeta) = \mathcal{F} + \upsilon\mathcal{F}\cos(2\theta)\cos(2\zeta). \tag{4.2-17}$$

While inscribing Bragg gratings in fibers, one tries to work in the linear regime where the photosensitivity of the fiber is proportional to the intensity of the UV

light. In this case the induced change Δn in the refractive index of the fiber is given as a function of ζ according to the following expression:

$$\boxed{\Delta n(\zeta) \propto 1 + \upsilon \cos(2\theta)\cos(2\zeta).} \tag{4.2-18}$$

This means that one induces refractive index variation with constant average level (no chirp) and apodization which is proportional to $\cos(2\theta)$. Thus, implementing computer control of the polarizer angle θ according to the position along the grating ζ, we are able to inscribe gratings with an arbitrary apodization as a function of ζ. Say, if we want to inscribe a grating with normalized apodization $A(\zeta)$, which is a slowly varying function of ζ compared to $\cos(2\zeta)$, then we have to vary the polarizer angle θ according to the following equation:

$$\boxed{\theta(z) = \pm\frac{1}{2}\arccos\left[A(z)\right].} \tag{4.2-19}$$

Here $|z| \leqslant L/2$ is position of the scanning UV beam along the grating and one can use either plus or minus sign.

Typical dependencies $\theta(z)$ are shown in Fig. 4.2 where normalized apodization function $A(z)$ is given by a Gaussian profile in Fig. 4.2-a) defined by equation

$$A(z) = \mathrm{G}_s(z) \equiv \exp\left\{-\ln 2\left[\frac{2(z - L/2)}{s \cdot L}\right]^2\right\}, \tag{4.2-20}$$

where L is the length of the grating and s is a *taper parameter* that describes the width of Gaussian profile and $|z| \leqslant L/2$. Fig. 4.2-b) shows a commonly used sinc -profile

$$A(z) = \mathrm{sinc}_s(z) \equiv \frac{\sin\left(\frac{2\pi z}{sL}\right)}{\left(\frac{2\pi z}{sL}\right)}, \quad |z| \leqslant L/2 \tag{4.2-21}$$

where sL is the spacing between the two central zero points $z_0 = \pm(s \cdot L)/2$. In some cases it can be desirable to superimpose these two types of apodization in order to reduce the so-called *Gibbs phenomenon* due to a finite length of the grating and hereby to improve some of its characteristics [83]. This situation is depicted in Fig. 4.2-c). In order for $\theta(z)$ to be smooth to reduce mechanical instability of the motor that controls angle θ one may choose to rewrite equation (4.2-19) as

$$\theta(z) = \frac{1}{2}\arccos[A(z)] \cdot \mathrm{sign}\, z, \tag{4.2-22}$$

where function

$$\mathrm{sign}\, z = \begin{cases} 1 & \text{for } z \geqslant 0, \\ -1 & \text{for } z < 0. \end{cases}$$

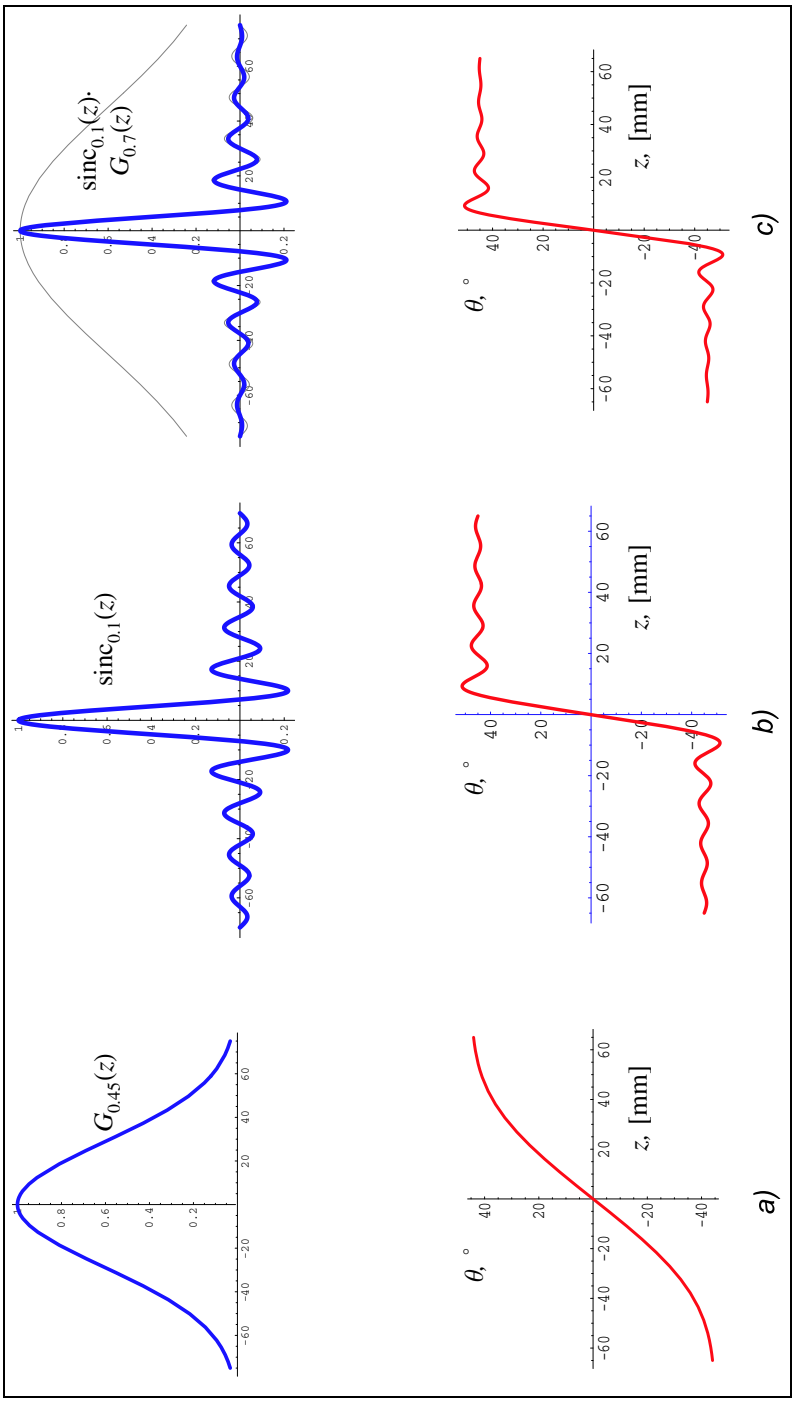

Figure 4.2: *Some most commonly used normalized apodization profiles $A(z)$ and their resulting $\theta(z)$ functions.* a) *Gaussian* b) *sinc and* c) *combined sinc- and Gaussian apodizations.*

In most practical cases though, we used equation (4.2-19) with positive sign for both negative and positive z in order to ensure that the used dependence of the UV power as a function of angle θ deviates as little as possible from the uniform distribution (see section 4.6). It is possible to introduce a π phase shift in apodization profile (or effectively negative apodization) by crossing the polarizer angle value of 45°.

4.2.4 Non-ideal situation

Equations (4.2-17) and (4.2-18) are valid in the case of the perfectly aligned experimental setup. When the values of the fiber-to-phase-mask distance and the polarizer angle deviate from the their optimal values, we get a slightly changed interference pattern and hereby refractive index change. In this case we have to use (4.2-15) with $\Delta\beta \neq 0$ and replace θ with $\theta_0 + \theta$, where θ_0 is a small misalignment angle and $\Delta\beta$ is given by equation (4.2-13). In the case of the perfect alignment the two position of the polarizer angle of 0 and 90° should give two different polarizations of the UV light on the fiber: one polarization along the fiber and the other perpendicular to the fiber. If $\theta \neq 0$, then we have a mixture of the two polarizations at $\theta = 0^\circ$ and $\theta = 90^\circ$. As in the ideal case, this inscribes a grating with constant average level of the refractive index change. As for the apodization of the grating, it will slightly modified compared to the ideal case. Equation (4.2-18) should be replaced by the following one:

$$\Delta n(\zeta) \propto 1 + \upsilon A(\theta)\cos(2\zeta + \beta_0), \tag{4.2-23}$$

where β_0 is a value depending on $\theta_0 + \theta$ and $\Delta\beta$

$$\tan\beta_0 = \frac{\sin^2(\theta_0 + \theta)\sin\Delta\beta}{\cos^2(\theta_0 + \theta) - \sin^2(\theta_0 + \theta)\cos\Delta\beta}, \tag{4.2-24}$$

and

$$A(\theta) = \sqrt{\cos^4(\theta_0 + \theta) - 2\cos^2(\theta_0 + \theta)\sin^2(\theta_0 + \theta)\cos\Delta\beta + \sin^4(\theta_0 + \theta)}. \tag{4.2-25}$$

In case when $\Delta\beta = \theta_0 = 0$ we get $\beta_0 = 0$ and $A(\theta) = \cos(2\theta)$ and equation (4.2-23) takes the form of the equation (4.2-18) as expected.

Equations (4.2-24) and (4.2-25) show that in case of imperfect adjustment of the polarizer angle ($\theta_0 \neq 0$ and $\Delta\beta = 0$), we induce an unchirped grating with a slightly different apodization profile than expected. While in case of imperfect alignment of the fiber-to-phase-mask distance ($\theta_0 = 0$ and $\Delta\beta \neq 0$) we get a change in the induced apodization profile as well and introduce an extra chirp in the grating ($\beta_0 \neq 0$). The introduced chirp β_0 is a function of the distance along the fiber z (or ζ) since both θ and $\Delta\beta$ depend on z:

$$\beta_0(z) = \beta_0\left(\theta(z), \Delta\beta\left(d_{\text{air}}(z)\right)\right).$$

4.3 Setup adjustment

Two important parameters of the experimental setup need careful adjustment in order to write gratings of high quality: polarizer angle (θ_0 must

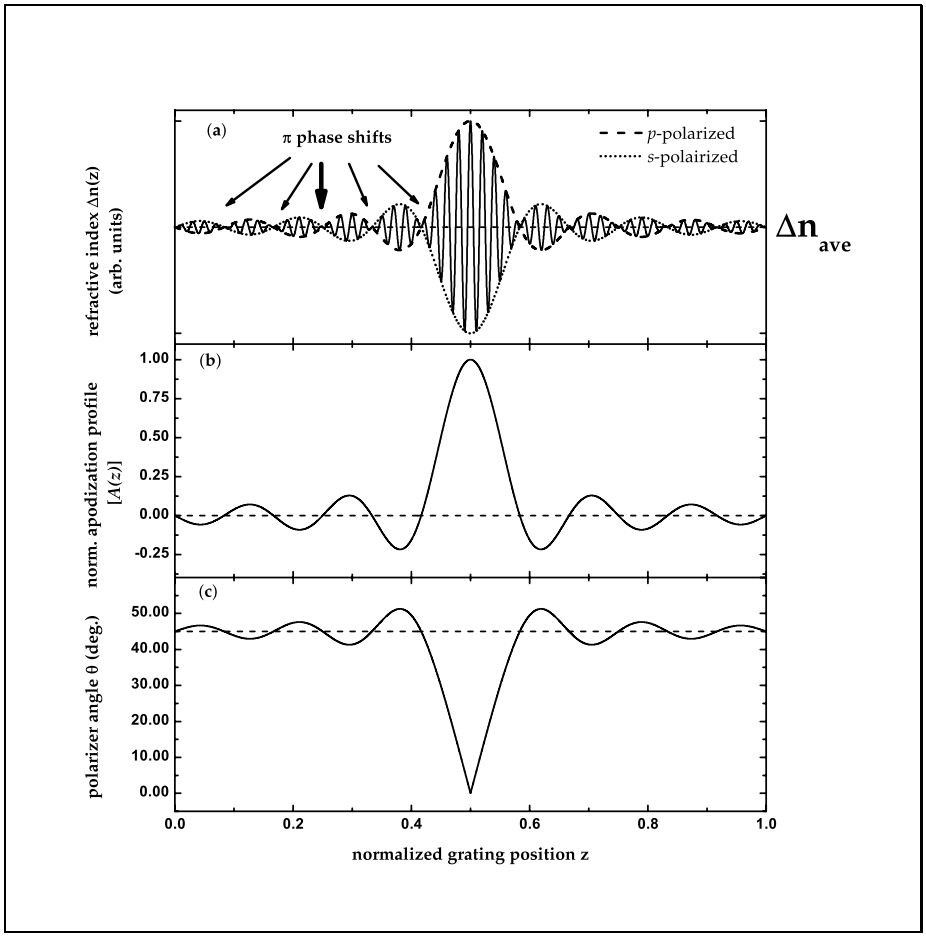

Figure 4.3: *(a) Schematic representation of the refractive index profile (solid line) of a sinc-apodized grating along with the normalized fluence profiles for p- and s-polarizations. The period is much smaller compared to the grating length. (b) Resulting apodization profile $A(z)$ and (c) corresponding polarizer angle $\theta(z) = 1/2 \arccos(A(z))$; the dashed line at the 45° level marks the cross-over between segments of the grating with different phase.*

be equal to 0) and fiber-to-phase-mask distance ($\Delta\beta$ should be equal to 0). Apodization profiles with multiple π phase shifts are especially sensitive to the proper setup adjustment. This allows us to choose such an apodization profile, e.g. a sinc-shaped apodization profile as a calibration profile which we can use in order to adjust the two important parameters of the setup optimally. Fig. 4.3 shows the chosen calibration sinc-shaped apodization profile with twelve π phase shifts.

The fiber-to-phase-mask distance is found experimentally by writing calibration weak sinc-like gratings (reflectivity $\sim 30\%$) with apodization profiles $A(z)$ given by

$$A(z) = \mathrm{sinc}_{1/6}(z) \cdot \mathrm{G}_7(z), \tag{4.3-1}$$

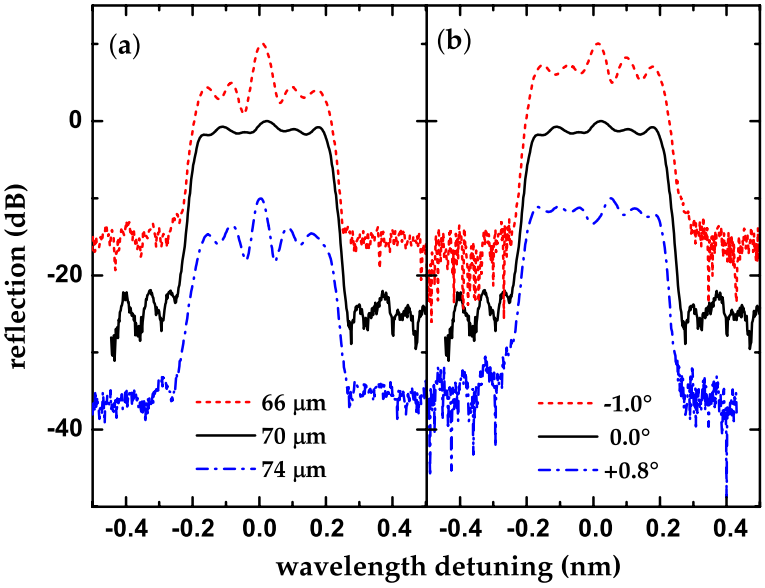

Figure 4.4: *(a) Calibration weak sinc-gratings written at different phase-mask-to-fiber distances at optimum polarizer angle. (b) Calibration weak sinc-gratings at different polarizer angle offsets. The resulting grating spectra are offset by* $\pm 10\,\mathrm{dB}$ *for clarity compared to the* $70\,\mu\mathrm{m}$ *and* 0.0° *respectively.*

where $\mathrm{sinc}_s(z)$ and $\mathrm{G}_s(z)$ are defined by equations (4.2-21) and (4.2-20). As known, the reflectivity spectrum of a weak sinc grating should have a rectangular profile. The deviations from this shape can be used as indication of how much the two critical parameters of the experimental setup deviate from their optimal values.

Thus, adjustment of the two parameters is an iterative process where the parameters are varied slightly with respect to their former values, then the obtained grating spectrum is compared to the predictions of the coupled mode theory with different values of the two parameters. In such a way one can get an idea about how much and in which direction one has to change the current values in order to adjust the setup optimally. Practical experience and computer simulations show that in order to write high quality Bragg gratings, one has to adjust the fiber-to-phase-mask distance with precision of about $1\,\mu\mathrm{m}$, while the polarizer angle position should not deviate more than 0.1° from its optimal value.

4.4 HNLF - highly nonlinear fiber

HNLF (the Highly Non-Linear Fiber) is a commercially available fiber from *OFS Denmark* optimized for use in non-linear devices. The fiber has a small effective area and a group velocity dispersion close to zero. Even though it is not especially designed for grating writing, we have found it to be well suited for this application. It has a high photosensitivity due to its highly Ge-doped core ($\sim 22\%\,\mathrm{Ge}$). The fiber has a complicated refractive index profile which is confidential and is not known to the users. In order to make computer simulation with any fiber, one has to know its characteristics such as its core radius, confinement factor, refractive indices of its core and cladding as a function of the distance from the fiber's center. Two known parameters of the HNLF fiber are the radius of its core $a = 1.181\,\mu\mathrm{m}$ and its confinement factor $\Gamma = 0.501$ [84].

We found out that one gets satisfactory simulation results if one assumes a *step index approximation* for this fiber, i.e. the refractive indices of the core n_{core} and the cladding n_{clad} are constant (independent of the distance from the fiber's center).

In order to determine the effective values of n_{core} and n_{clad}, a 3 mm long test uniform grating has been written in HNLF and development of its spectrum has been monitored with time. Measuring the transmittivity spectrum during the exposure, we hereby determine the position and the strength of the transmittivity dip as a function of time (or total UV light fluence). Using these data and coupled mode theory, one can calculate the dependencies of the effective refractive index n_{eff} and the modulation strength Δn of the grating as functions of time (or total UV fluence F), that are illustrated in Fig. 4.5. One can

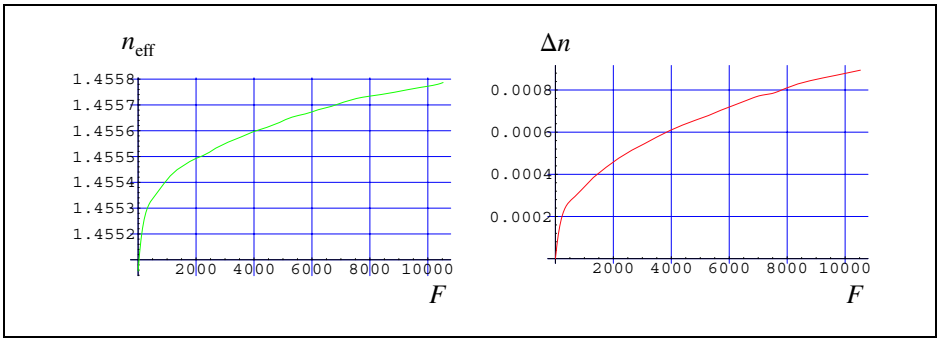

Figure 4.5: *Effective refractive index n_{eff} and modulation strength Δn as functions of UV-light fluence F [J/cm^2] for a 3 mm long uniform Bragg grating in HNLF (highly non-linear fiber).*

see that the effective refractive index of this fiber in the absence of the grating is equal to

$$n_{\text{eff}} = \lim_{F \to 0} \left[n_{\text{eff}}(F) \right] = 1.4551.$$

The coupled mode theory gives theoretical expressions for the confinement factor Γ and effective refractive index n_{eff} as functions of n_{core}, n_{clad} and the radius of the fiber's core a as defined by equations (3.1-18) and (3.1-20):

$$\begin{cases} \Gamma\left(n_{\text{core}}, n_{\text{clad}}, a\right) = 0.501, \\ n_{\text{eff}}\left(n_{\text{core}}, n_{\text{clad}}, a\right) = 1.4551. \end{cases} \tag{4.4-1}$$

Knowing the value of a to be equal to $1.181\,\mu\text{m}$, we can readily find the numerical values of n_{core} and n_{clad} [85]:

$$\boxed{\begin{array}{l} n_{\text{core}} = 1.4823, \\ n_{\text{clad}} = 1.4460. \end{array}} \tag{4.4-2}$$

These values of n_{core} and n_{clad} are used in all computer simulations in this thesis together with the step index approximation.

4.5 Birefringence

Birefringence is a difference in photosensitivity of an optical fiber to two different polarizations of the UV light [86]. This induced birefringence can be harmful for optical devices such as grating based optical filters [87]. On

the other hand, birefringence can be useful for controlling the polarization of a single-mode distributed feed back (DFB) fiber laser [88].

One can find a broad discussion in the literature about the origin of the birefringence in the optical fibers. There are at least four contributions to it:

- a geometric asymmetry of the index change is induced because of the finite penetration depth of the UV light. This effect is complicated by the high variability in the excimer UV intensity per pulse, preventing a uniform index change across the core [89, 90];
- the dipole orientation when working with polarized UV light [91, 92];
- differences in scattering between the two polarization states of the writing laser as a result of the circular geometry of both the outer cladding and the core-cladding interface;
- relationship between densification along the laser writing axis [93] and the stress release along this axis [87, 94].

These four effects and the interplay between them are very controversial in literature and have not been satisfactorily studied. The presented polarization control method uses both the s- and the p-polarization state of the UV light, while inscribing a Bragg grating and *may* induce significant birefringence into the target apodization profile.

To check the presence and the magnitude of the birefringence in the used HNLF fiber, we performed experiments similar to Erdogan and Mizrahi where the experimental setup is described in details [89–91]. Briefly, uniform excimer laser radiation (UV wavelength $248\,\mathrm{nm}$) was incident upon a deuterium-loaded HNLF fiber. A commercial polarization analyzer (HP8509B) consisting of a laser source of $\lambda = 1530\,\mathrm{nm}$ and a set of three polarizers (aligned 60° with respect to each other) was used to measure the growth in birefringence of the fiber.

It can be shown [91] that if $\mathbb{T}(t)$ denotes the Jones matrix of the fiber section being exposed at time t, measured by the polarization analyzer, then the birefringence Δn_{br} of the fiber can be calculated by

$$\boxed{\Delta n_{\mathrm{br}} = \frac{\lambda}{2\pi L}\left|\arg\left(\Lambda_1\right) - \arg\left(\Lambda_2\right)\right|,} \tag{4.5-1}$$

where $\lambda = 1530\,\mathrm{nm}$, L is the length of the exposed part of the fiber, $\arg(z)$ is the argument of the complex number z. The parameters Λ_1 and Λ_2 are the complex eigenvalues of the matrix $\mathbb{T}(t)\mathbb{T}^{-1}(0)$, i.e. the two solutions to the following equation

$$\det\left[\mathbb{T}(t)\mathbb{T}^{-1}(0) - \Lambda \cdot \mathbb{I}\right] = 0, \tag{4.5-2}$$

where $\mathbb{I}$ is the identity matrix.

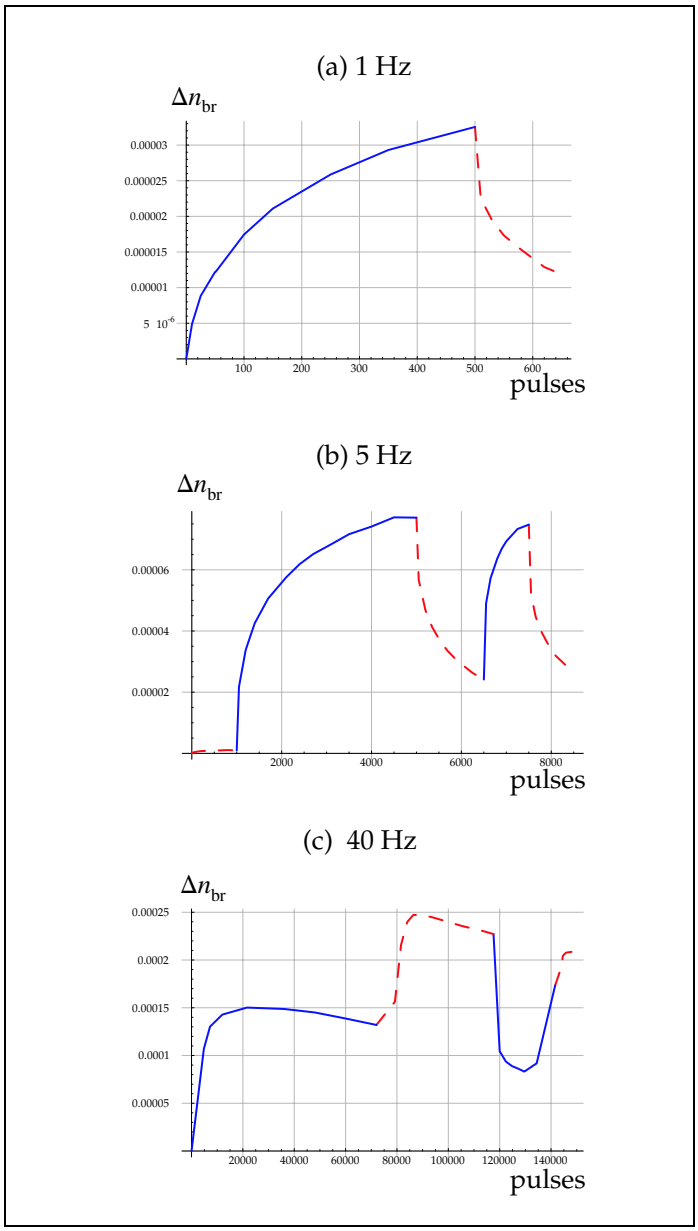

Figure 4.6: *Induced birefringence in deuterium loaded HNLF as a function of the number of UV light pulses (one pulse fluence* 36 mJ/cm^2 *) with different pulse rates of the laser (a)* 1 Hz *, (b)* 5 Hz *and (c)* 40 Hz *. A solid blue line depicts exposure by* s *-polarized light, and a dashed right line – p -polarized light.*

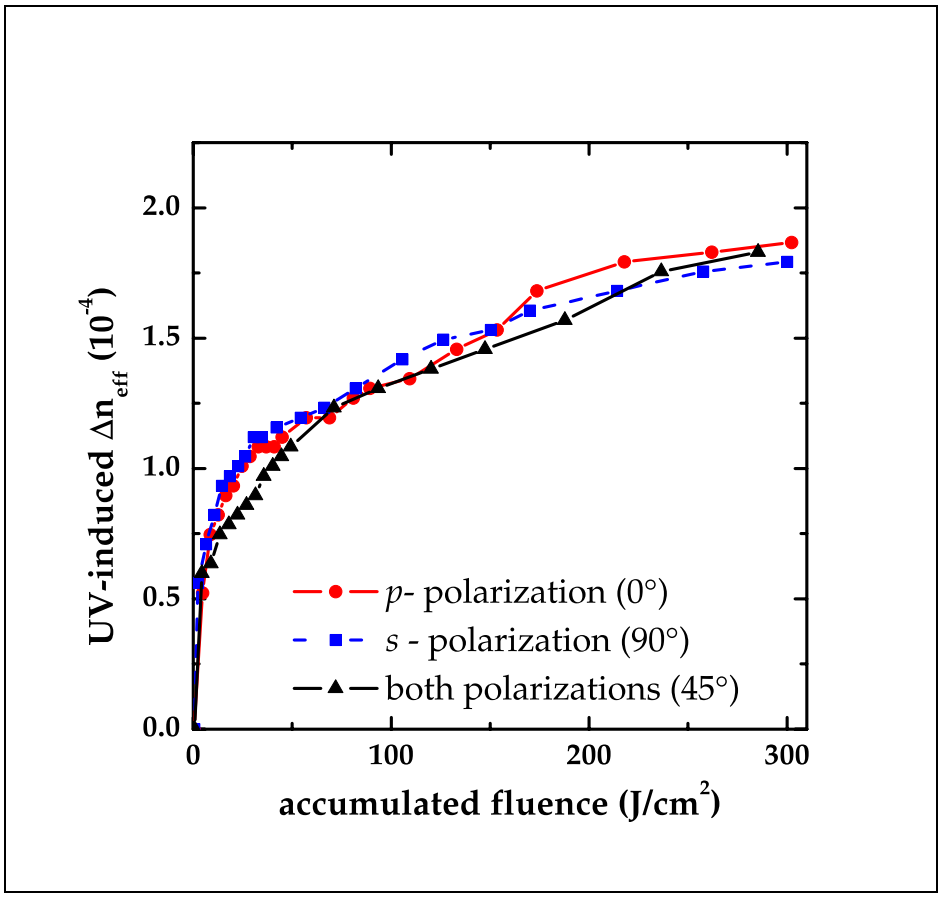

Figure 4.7: *The UV-induced effective index change in pristine (not loaded) HNLF fiber as a function of the accumulated fluence for different polarizations. Error bars are not included for clarity. The measurement uncertainty is* $\pm 2\%$ *.*

A $L = 0.7\,\text{mm}$ long piece of HNLF has been exposed to the 248 nm excimer laser UV light. Fluence of one pulse of the UV light was measured to be $36\,\text{mJ/cm}^2$. Fig. 4.6 shows the experimental results of birefringence measurements at three different pulse rates of the 248 nm excimer laser of 1 Hz, 5 Hz and 40 Hz. We can see in Fig. 4.6-(b) and (c) that at those values of UV fluence that are normally used for Bragg grating inscription (up to a couple of kJ/cm^2), the induced birefringence is very sensitive to s-polarized UV light ($\theta = 90^\circ$) and can be reduced by a second exposure with p-polarized light ($\theta = 0^\circ$). This is consistent with experimental results of other authors [87,88,91]. We have ob-

served that in all cases the induced birefringence is not larger than $2-3\%$ of the total induced refractive index change.

Thus, these results suggest, that by writing gratings in deuterium loaded HNLF fiber with mainly p-polarized light and a post treatment with $5-10\%$ of the initial UV dose in p-polarization, we can fabricate highly isotropic fiber Bragg gratings using the polarization control method. Using a CW laser operating in the long-wavelength tail of the 266 nm absorption will suppress the induced birefringence significantly [90,94].

Fig. 4.6-(c) represents an interesting case of a very high value of UV fluence of about $5\,\mathrm{kJ/cm^2}$ which is typically not used for Bragg grating inscription. Nevertheless, the graph confirms one again that birefringence is a very complicated phenomenon and should studied and be taken into account during UV inscription of advanced Bragg gratings. A comprehensive study of birefringence could be desirable and very interesting but it is beyond the scope of this thesis.

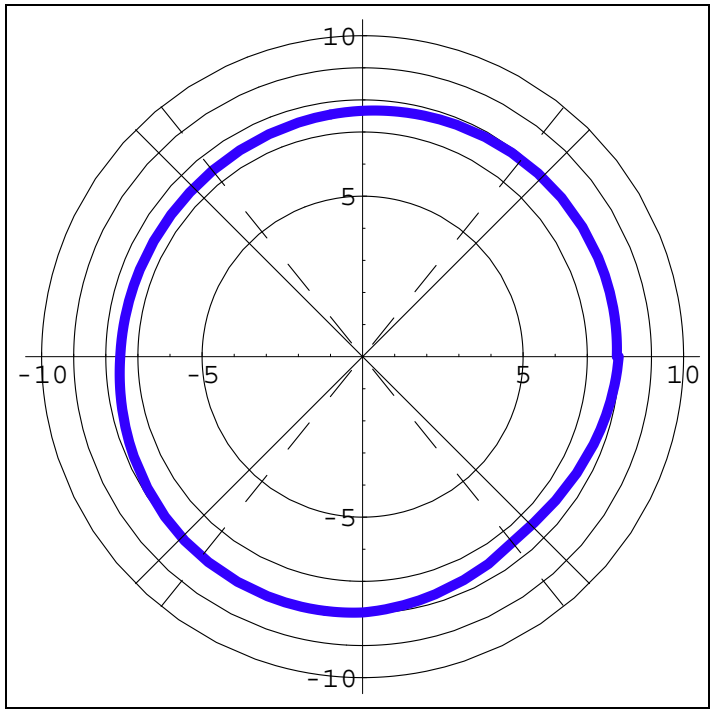

Figure 4.8: *A typical UV intensity* (mJ/cm^2/pulse) *angular distribution used in polarization control method. It is uniform with precision of* $1-2\%$ *in the working interval from zero to* 50°.

In order to be sure that the polarized UV light induces the same refractive index change independent of its polarization, we have written several similar uniform grating at different constant angles of the UV light polarizer. The result is shown in Fig. 4.7 where the results for three similar uniform gratings are presented. One can see that both polarizations induce the same refractive index change within the measurement uncertainty.

4.6 UV intensity angular distribution

As mentioned before we used a tilted quartz plate in order to equalize the UV power output in both polarizations. By changing the angle between the plate and the direction of the UV beam, we can experimentally find the angle that ensures a uniform angular distribution of the UV intensity.

Actually, the the angular distribution does not need to be uniform for all angles. As we can see in Fig. 4.3 the polarizer angle changes only from zero to $\sim 50^{\circ}$ and it needs to be uniform only in this interval. Fig. 4.8 shows a typical angular distribution of the UV light power. It is uniform in the interval of interest with precision of $1-2\%$.

Chapter 5

Bragg grating design

Wide-spread usage of Bragg gratings in optical communication systems requires techniques capable of designing gratings with specific properties, i.e. to synthesize the *coupling coefficient* from the desired spectral response. Various approaches, both iterative and non-iterative, exist at the present time [39, 95–97]. The earliest synthesis methods used the *Gel'fand-Levitan-Marchenko inverse scattering algorithm* [98] which is based on iterative solution of an integral equation in order to get the whole grating profile. Later, an iterative and general technique was developed [99]. A couple of alternative techniques such as *differential inverse scattering algorithm* [100], *signal processing technique* [101] and *evolutionary synthesis* [102] have been proposed lately. The *layer-peeling algorithm* [96] is a commonly used non-iterative differential method that is used to extract the grating profile sequently section by section.

Differential methods of grating design have proven to be more effective compared to the integral ones when considering computational speed and accuracy of reconstruction. An intrinsic part of these methods is an artificial but inevitable modification of a generally non-casual impulse response of the desired grating by a windowing procedure. As a result the spectral response of the constructed grating might deviate considerably the desired one. The effect becomes more pronounced in case of short and strong gratings which are attractive due to their compactness and easy manufacturing.

Poladian suggested a very simple and elegant grating synthesis algorithm [103]. It utilizes the direct solution of exactly the same *coupled mode equations* that are used in grating analysis, thus it has a transparent description which is not obscured by the underlying mathematical formalism. The complex *coupling coefficient* $q(z)$ encodes all the information about the *apodization* and *chirp* of the grating and is given as a function of the distance z along the grating according to the simple *synthesis relation*:

$$q(z) = \frac{2i}{\pi} \int_{-\infty}^{\infty} r^*(z, \delta)\, d\delta, \tag{5.0-1}$$

where the *detuning* δ is proportional between the and the Bragg frequencies and $r(z, \delta)$ is a *partial reflection coefficient* obtained from solving the coupled-mode equations while simultaneously evaluating $q(z)$ using equation (5.0-1). Simple and smart as it is, this technique produces complicated chirped grating profiles that are difficult and expensive to fabricate and may require a custom-made phase mask with a complicated non-uniform profile. The same disadvantage takes place for the layer-peeling method despite the fact that it can be modified into a combination of integral and differential methods in order to deal with the problem of designing strong gratings [104].

Most of the existing techniques are either capable of designing a restricted class of gratings or are slow and ineffective, especially for strong gratings. We suggested a new iterative approach for designing Bragg gratings [105, 106]. It is based on minimizing a χ^2 merit function using *Levenberg-Marquardt* (LM) method (also called *Marquardt method*) [107–109], i.e. minimizing the discrepancy between the target spectral response and the spectral response of the reconstructed grating via nonlinear *least-square minimization*, where the discrepancy is presented as a multi-variable of the discretized grating profile. Despite nonlinear least square minimization has a long history, it has not been applied for optimization of grating designs before. The method we suggest is highly efficient due to the possibility of analytical calculation of the gradient of the merit function and invoking iterative schemes into the optimization process.

The number of calculational operations with respect to the number of the variables N for the LM method is estimated to $O(N^2 \log(N))$ which is comparable to the quickest of the existing inverse scattering solvers as far as the complexity of the algorithm is concerned. Nevertheless, it is much quicker than any other existing method due to the fact that it does not use the *fast Fourier transform* and hence is much less limited by finite bandwidth and resolution of the target spectrum. This allows choosing much fewer sampled points along the spectrum and the grating, thus providing less calculation time.

The method is effective for both strong and weak gratings along their whole length. The second important advantage is that one can choose to design *unchirped gratings* with specified spectral properties. This type of gratings are very easy to fabricate with our recently developed *polarization control method* [63] which is developed for fabricating Bragg gratings with arbitrary *apodization* (amplitude of the *coupling coefficient*) but no *chirp* (phase of the grating's *coupling coefficient*).

5.1 Levenberg-Marquardt algorithm

The *Levenberg-Marquardt method* has become the standard for implementing nonlinear least-squares routines. It was developed by Marquardt [109], related to an earlier suggestion of Levenberg [108]. Before this method (also

called *Marquardt method*) has been developed, it was common to use a *Taylor series* for a non-linear problem and to make correction to a solution achieved during previous iteration on the assumption of local linearity. On the other hand, several modifications of the *method of steepest descent* (or gradient) have been used. Both of them frequently did not lead to a desired result either because of slow convergence or divergence.

The *Marquardt method* which is sometimes called a *maximum neighborhood method* performs an optimum interpolation between the Taylor series and the gradient method, the interpolation being based upon the maximum neighborhood in which the truncated Taylor series gives an adequate representation of the non-linear model. The latter method is used far from the minimum, switching continuously to the former as the minimum is approached [107].

We consider a function

$$y = y(x, \mathbf{a}), \tag{5.1-1}$$

that depends on a set of N parameters $\mathbf{a} = (a_1, a_2, \ldots a_N)$. The merit function $\chi^2(\mathbf{a})$ is defined in the following way:

$$\boxed{\chi^2(\mathbf{a}) = \sum_{i=1}^{M} \left[\frac{y_i - y(x_i, \mathbf{a})}{\sigma_i} \right]^2.} \tag{5.1-2}$$

Here $\mathbf{x} = (x_1, x_2, \ldots x_M)$ is a set of points where the function $y(x, \mathbf{a})$ is to be fitted by the values $\mathbf{y} = (y_1, y_2, \ldots y_M)$ with uncertainties $\boldsymbol{\sigma} = (\sigma_1, \sigma_2, \ldots \sigma_M)$. Our task here is to find a set of parameters $\mathbf{a}$ that minimize $\chi^2(\mathbf{a})$ from equation (5.1-2). With nonlinear dependencies the minimization must proceed iteratively. Given trial values for the parameters, the *Marquardt method* suggests a procedure that improves the trial solution. The procedure is then repeated until χ^2 stops (or effectively stops) decreasing.

Sufficiently close to the minimum, we expect the χ^2 function to be well approximated by a quadratic form and according to the *steepest descent (gradient) method* we can proceed from the current iteration $\mathbf{a}_{\text{cur}}$ to the next iteration $\mathbf{a}_{\text{next}}$ in the following way:

$$\mathbf{a}_{\text{next}} = \mathbf{a}_{\text{cur}} - A \nabla\chi^2(\mathbf{a}_{\text{cur}}), \tag{5.1-3}$$

where $A = \text{const}$ is a constant value and $\nabla\chi^2(\mathbf{a}_{\text{cur}})$ is a gradient of χ^2 at the set of parameters $\mathbf{a}$. This equation is equivalent to

$$\delta a_l = A \beta_l, \quad \text{for} \quad l = 1, 2, \ldots N, \tag{5.1-4}$$

where δa_l is a change in parameter with number l and β_l is the $l-$ th component of the gradient of $\chi^2(\mathbf{a})$:

$$\beta_l = \frac{1}{2} \frac{\partial \chi^2}{\partial a_l}. \tag{5.1-5}$$

The *Marquardt method* is based on two elementary, but important, insights. Consider the "constant" A in equation (5.1-4). What should it be, even in order of magnitude? What sets its scale? There is no information about the answer in the gradient. That tells only the slope, not how far that slope extends. Marquardt's first insight is that the components of the Taylor series, even if they are not usable in any precise fashion, give some information about the order-of-magnitude scale of the problem. The equation (5.1-5) should be replace by the following equation

$$\delta a_l = \frac{\beta_l}{\lambda \alpha_{ll}}, \tag{5.1-6}$$

where α_{lk} is a coefficient in the Taylor series of $\chi^2(\mathbf{a})$:

$$\alpha_{kl} = \sum_{i=1}^{M} \frac{1}{\sigma_i^2} \left[\frac{\partial y(x_i, \mathbf{a})}{\partial a_k} \frac{\partial y(x_i, \mathbf{a})}{\partial a_l} \right] \tag{5.1-7}$$

and λ is a dimensionless parameter.

Marquardt's second insight was to define a new matrix α' in the following way:

$$\begin{cases} \alpha'_{kl} = \alpha_{kl} & \text{for} \quad k \neq l, \\ \alpha'_{ll} = \alpha_{ll}(1 + \lambda), \end{cases} \tag{5.1-8}$$

and replace (5.1-6) by the following equation:

$$\sum_{l=1}^{N} \alpha'_{kl} \delta a_l = \beta_k. \tag{5.1-9}$$

When λ is very large, equation (5.1-9) reduces to the (5.1-6) that represents the *steepest descent method* but on the other hand as λ approaches zero the given equation leads to

$$\sum_{l=1}^{N} \alpha_{kl} \delta a_l = \beta_k,$$

which represents the *Taylor series method* [109].

Given an initial guess for the set of fitted parameters $\mathbf{a}$, the recommended Marquardt recipe is as follows:

① compute $\chi^2(\mathbf{a})$,

② pick a modest value for λ say $\lambda = 0.001$,

③ solve the linear equations (5.1-9) for $\delta\mathbf{a}$ and evaluate $\chi^2(\mathbf{a} + \delta\mathbf{a})$,

④ if $\chi^2(\mathbf{a} + \delta\mathbf{a}) \geqslant \chi^2(\mathbf{a})$, *increase* λ by a factor of 10 (or any other substantial factor) and go back to ③,

⑤ if $\chi^2(\mathbf{a}+\delta\mathbf{a}) < \chi^2(\mathbf{a})$, *decrease* λ by a factor of 10, update the trial solution $\mathbf{a} \leftarrow \mathbf{a}+\delta\mathbf{a}$, and go back to ③.

It is also necessary to have a condition for stopping. Iterating to machine accuracy is generally wasteful and unnecessary. In practice, one might as well stop iterating on the first or second occasion that χ^2 decreases by a negligible amount. One must not stop after a step where χ^2 increases, this only shows that λ has not yet adjusted itself optimally.

Thus, in order to implement the *Marquardt method*, one should have both values of function $y(\mathbf{a})$ (5.1-1) and its derivatives used in equations (5.1-5) and (5.1-7). The next section describes the use of the *Marquardt method* for Bragg grating design.

5.2 Marquardt method for Bragg grating design

The iterative procedure of the method is based on calculation of the spectral characteristics of the grating given its refractive index modulation $n_{\text{eff}}(\zeta)$ from equations (1.3-7) and (3.1-22). Since we design the gratings in order to fabricate them using the *polarization control method*, we can assume $\sigma(\zeta) \equiv \sigma = \text{const}$ in equation (3.1-22) since the *polarization control method* gives $n_{\text{ave}}(\zeta) = \text{const}$ (*see* section 4.1) for the DC component of the refractive index change in the fiber's core.

We use the *transfer matrix method* described in section 3.6. We divide the existing length of the grating L (or $\zeta_L \equiv k_0 L$) by N points placed at equal distance Δz (or $\Delta\zeta \equiv k_0 \Delta z$) to each other and hereby we sample the function $n_{\text{mod}}(z)$ by its values at these points z_i, where $i = 1, 2, \ldots N$. At every interval

$$|z - z_i| < \Delta z/2$$

we assume the apodization function $n_{\text{mod}}(z)$ to be constant and equal to $n_i = n_{\text{mod}}(z_i)$. The *transfer matrix method* supplies a procedure for calculating the spectral characteristics of the the whole grating knowing complex values of transmission and reflection coefficients of its uniform parts. The latter are given by simple equations of the *coupled-wave theory* described in section 3.2.

Thus, one can calculate spectral properties of the grating given the values

$$\mathbf{n} = (n_1, n_2 \ldots n_i \ldots n_N), \tag{5.2-1}$$

which are being optimized by the *Marquardt method* in a succession of iterations in order to minimize the discrepancies between the current calculated values of the grating's spectral functions and their desired values.

The spectrum can be discretized with M sampling points over a finite bandwidth $\Delta\omega$ (or $\Delta\delta = n_{\text{eff}}\Delta\omega/c$) that we are interested in, with a sampling

frequency of $d\omega$ (or $d\delta = n_{\text{eff}} d\omega / c$). Since we are interested only in spectrum in the vicinity of the *central frequency* ω_c which corresponds to the *central wavelength* λ_c given by equation (4.2-1)

$$\omega_c = \omega_0 (1 - \sigma),$$

we can choose to use $\hat{\sigma}$ as the spectrum variable (instead of δ or wavelength λ) with the center in ω_c. Thus, the spectrum points that we choose are given by M values of the parameter $\hat{\sigma}$ with center in $\hat{\sigma} = 0$ (corresponding to ω_c) and interval of $d\hat{\sigma} = d\delta$ between two adjacent points

$$\hat{\boldsymbol{\sigma}} \equiv (\hat{\sigma}_1, \hat{\sigma}_2 \ldots \hat{\sigma}_M). \tag{5.2-2}$$

5.2.1 Choice of initial set of parameters

The choice of the initial set of values $\mathbf{n_0}$ is crucial for obtaining the final optimized result. It is important to start sufficiently close to the *global minimum* to avoid ending up in a *local minimum*. According to our experience, a *Fourier transform* of the target reflectivity spectrum or its part makes a good start guess and leads to an acceptable convergence. Thus, if we want to design a spectrum which has a rectangular-shaped reflectivity profile, we can choose a truncated sinc-profile for an initial set of variables $\mathbf{n_0}$. One should though normalize the obtained $\mathbf{n_0}$ set of variables before use, so that they ensure the appropriate strength of the grating in transmittivity close to the transmittivity of the target spectrum.

5.3 Spectral functions and their derivatives

In order to calculate values of the spectral functions of the grating and their derivatives, we use the *transfer matrix method* described in section 3.6. According to equation (3.6-9) we have:

$$\hat{\mathbf{T}}^{-1} = \prod_{i=1}^{N} \left(\hat{\mathbf{T}}^{-1}\right)_i = \prod_{i=1}^{k-1} \left(\hat{\mathbf{T}}^{-1}\right)_i \cdot \left(\hat{\mathbf{T}}^{-1}\right)_k \cdot \prod_{i=k+1}^{N} \left(\hat{\mathbf{T}}^{-1}\right)_i, \tag{5.3-1}$$

for any $k = 1, 2 \ldots N$ if we define the following products to be equal to the unity 2×2 matrix $\mathbb{I}$

$$\prod_{i=1}^{0} \left(\hat{\mathbf{T}}^{-1}\right)_i = \prod_{i=N+1}^{N} \left(\hat{\mathbf{T}}^{-1}\right)_i \equiv \mathbb{I}.$$

In this way the transfer matrix $\hat{\mathbf{T}}^{-1}$ of the whole grating is equal to the product of three parts:

❶ the first (left) part denoted $\mathbb{L}$ which is independent of the current number k and value n_k

$$\mathbb{L} \equiv \left[\!\!\left[\begin{array}{cc} L_{1,1} & L_{1,2} \\ L_{2,1} & L_{2,2} \end{array} \right]\!\!\right] \equiv \prod_{i=1}^{k-1} \left(\hat{\mathbf{T}}^{-1}\right)_i, \tag{5.3-2}$$

❷ the second (central) part denoted $\mathbb{C}$ which depends on n_k through the matrix $\left(\hat{\mathbf{T}}^{-1}\right)_k$ as specified by equation (3.6-4), where k_k depends on n_k as defined in (1.2-3)

$$\mathbb{C}(n_k) = \left(\hat{\mathbf{T}}^{-1}\right)_k \equiv \left[\!\!\left[\begin{array}{cc} C_{1,1}(n_k) & C_{1,2}(n_k) \\ C_{2,1}(n_k) & C_{2,2}(n_k) \end{array} \right]\!\!\right], \tag{5.3-3}$$

here $C_{i,j}(n_k)$ for $i, j = 1, 2$ are known analytical functions of their argument defined in equation (3.6-4),

❸ the third (right) part denoted $\mathbb{R}$ which is independent of the value n_k

$$\mathbb{R} \equiv \left[\!\!\left[\begin{array}{cc} R_{1,1} & R_{1,2} \\ R_{2,1} & R_{2,2} \end{array} \right]\!\!\right] \equiv \prod_{i=k+1}^{N} \left(\hat{\mathbf{T}}^{-1}\right)_i. \tag{5.3-4}$$

As a result we can write the following equation using equation (3.6-8) for the transfer matrix $\hat{\mathbf{T}}^{-1}$

$$\hat{\mathbf{T}}^{-1} = \left[\!\!\left[\begin{array}{cc} 1/t & \left(r^{+}/t\right)^{*} \\ r^{+}/t & 1/t^{*} \end{array} \right]\!\!\right] = \mathbb{L} \cdot \mathbb{C}(n_k) \cdot \mathbb{R},$$

or combined with equations (5.3-2), (5.3-3) and (5.3-4) we have

$$\left[\!\!\left[\begin{array}{cc} 1/t & \left(r^{+}/t\right)^{*} \\ r^{+}/t & 1/t^{*} \end{array} \right]\!\!\right] = \left[\!\!\left[\begin{array}{cc} L_{1,1} & L_{1,2} \\ L_{2,1} & L_{2,2} \end{array} \right]\!\!\right] \cdot \left[\!\!\left[\begin{array}{cc} C_{1,1}(n_k) & C_{1,2}(n_k) \\ C_{2,1}(n_k) & C_{2,2}(n_k) \end{array} \right]\!\!\right] \cdot \left[\!\!\left[\begin{array}{cc} R_{1,1} & R_{1,2} \\ R_{2,1} & R_{2,2} \end{array} \right]\!\!\right]. \tag{5.3-5}$$

Multiplying the three matrices in the right part of the equation (5.3-5) and comparing the resulting 2×2 matrix to the matrix in the left side of the equation, we get the theoretical expressions for complex spectral functions of the grating such as its transmission $t(n_k)$ and reflections from both sides $r^{+}(n_k)$ and $r^{-}(n_k)$ as functions of the current n_k from the set of variables $\mathbf{n}$. One can for example easily get an expression for $t(n_k)$:

$$t(n_k) = \left[R_{1,1}\left(L_{1,1}C_{1,1}(n_k) + L_{1,2}C_{2,1}(n_k)\right) + R_{2,1}\left(L_{1,1}C_{1,2}(n_k) + L_{1,2}C_{2,2}(n_k)\right)\right]^{-1}, \tag{5.3-6}$$

and similar expression for $r^+(n_k)$:

$$r^+(n_k) = \frac{R_{1,1}\left(L_{2,1}C_{1,1}(n_k) + L_{2,2}C_{2,1}(n_k)\right) + R_{2,1}\left(L_{2,1}C_{1,2}(n_k) + L_{2,2}C_{2,2}(n_k)\right)}{R_{1,1}\left(L_{1,1}C_{1,1}(n_k) + L_{1,2}C_{2,1}(n_k)\right) + R_{2,1}\left(L_{1,1}C_{1,2}(n_k) + L_{1,2}C_{2,2}(n_k)\right)}. \quad (5.3\text{-}7)$$

The last two equations give analytical expressions for transmission t and reflection r^+ as functions of the value of the refractive index n_k of the uniform part with number k. All other spectral functions such as transmittivity T, reflectivity R, dispersion d and group delay D can be analytically calculated from these two as described in section 3.5. Moreover, since all the functions $C_{i,j}(n_k)$ are known analytical functions, we can analytically calculate the derivatives of all the spectral functions we are interested in as functions of all values n_k for $k = 1, 2\ldots N$.

As a example, one could wish to design a Bragg grating with a certain logarithmic transmittivity $\mathcal{T}$ which is defined by

$$\mathcal{T} = 10\log_{10}\left(|t|^2\right). \quad (5.3\text{-}8)$$

Equation (5.3-6) gives dependence of $\mathcal{T}$ on any arbitrary n_k:

$$\mathcal{T}(n_k) = 10\log_{10}\left(t(n_k)t^*(n_k)\right).$$

Using this expression, it is straightforward to calculated to derivative $\mathcal{T}'(n_k)$. It can be written as

$$\mathcal{T}'(n_k) = \frac{20}{\ln 10}\,\mathfrak{Re}\left(\frac{t'(n_k)}{t(n_k)}\right), \quad (5.3\text{-}9)$$

where $\mathfrak{Re}(z)$ is a real part of a complex number z. In order to define derivatives of such spectral functions of group delay and dispersion, we need the derivative of the transmission's phase $\phi_t(n_k)$ as a function of any arbitrary n_k. It can be found in a way similar to equation (5.3-9):

$$\phi_t'(n_k) = \mathfrak{Im}\left(\frac{t'(n_k)}{t(n_k)}\right), \quad (5.3\text{-}10)$$

where $\mathfrak{Im}(z)$ is an imaginary part of a complex number z.

5.3.1 Beauty of the spectral derivatives

One can draw beautiful color pictures if one plots the dependencies of the derivatives of the spectral functions in color with different colors changing from blue for low values to red for higher values. If we consider for instance logarithmic transmittivity $\mathcal{T}$ as a function of both k (a number of a uniform part of the grating along the its length) and m (a number along the discretized

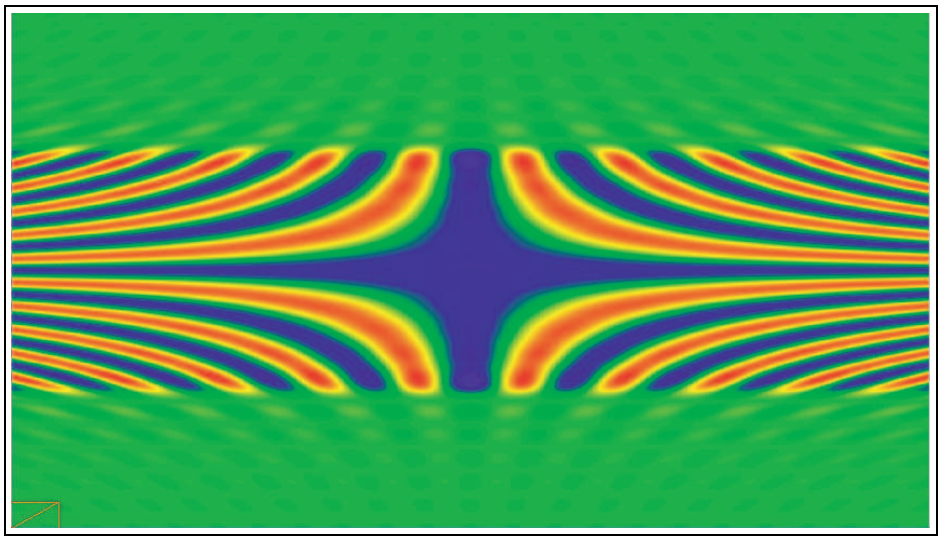

Figure 5.1: *Derivative Υ of a Bragg grating with a sinc-shaped apodization profile.*

grating's spectrum given by (5.2-2)), then we can draw $\Upsilon(k, m)$ as a 2D plot with different colors for different values of the calculated derivative $\Upsilon'(k, m)$.

An example of such a plot is used on the cover page of the thesis. it was plotted for a uniform Bragg grating written in HNLF fiber with the length of 23 mm and apodization strength of $7.5 \cdot 10^{-5}$. The horizontal axis in the plot defines the direction of the grating and the vertical axis varies along the frequency of the grating's spectrum (in the vicinity of the grating's central wavelength λ_c).

Another beautiful plot is shown in Fig. 5.1 for a sinc-shaped grating. The grating is 23 mm long with a maximum of apodization strength of $5 \cdot 10^{-4}$.

5.4 Fitting multiple spectral characteristics

The described algorithm can easily be generalized to the case when one wants to fit several spectral functions of the grating simultaneously. For example, if one wants to design a grating with specific dependencies for reflectivity $R(\omega)$ and group delay in reflection $D_r(\omega)$. One simply has to combine the two spectral functions into one generalized function $Q(\omega)$. In this case the number of sampling points along the new generalized spectrum gets twice as large as before, i.e. $2M$. Now, if we define $Q_i \equiv R(\mathbf{n})$ and $Q_{i+M} \equiv D_r(\mathbf{n})$ for

$i = 1, 2 \ldots M$, we can use the same algorithm for minimizing the value of χ^2 which in this case is defined in the same way as in equation (5.1-2) except that M should be replaced by $2M$.

It is of course the user's own responsibility not to impose some non-physical restrictions on the target's spectral characteristics and their self-consistency. One should remember that the spectral functions of the grating are not independent of each other but are connected by relations described in section 3.5.

Chapter 6

Examples and results

6.1 Single channel filter examples

The remarkable ability of the described design algorithm is that one is free to fix some parameters of the grating during the iteration process and thereby to decide in advance what those values will be in the final design. So one can decide before designing a grating that it should have a certain length L or, if necessary, choose it to be symmetric with respect to its center. In the latter case one should choose only half of all the values $\mathbf{n}$ as the parameters to be optimized during the iteration process while the other half is assumed to be equal to them. This is also a reason why it is easy to design unchirped gratings. One simply assumes from the beginning that $n_{\text{ave}}(z)$ = const and $\varphi(z)$ = const and keeps this condition fixed during execution of the fitting algorithm. Imposing additional constraints (such as grating length, symmetry, or absence of chirp) makes the design results more practical. Unchirped grating have simple apodization without imaginary part (*chirp*) and are easy to fabricate with existing method such as our polarization control method.

A grating shown in Fig. 6.1-(a) represents a grating designed to have a rectangular filter function transmittivity profile with $-40\,\text{dB}$ signal suppression. It was written in a D_2-doped HNLF fiber. Negative values of the grating's apodization mean the phase shift of π in the grating's structure.

Another grating is shown in Fig. 6.1-(b). It has been designed to be symmetric and to have a rectangular reflectivity profile with $\sim$ 30 dB side lobe suppression as well as constant group delay $D_r^+(\omega)$ (as far as it is possible for a symmetric grating). Both profiles show excellent agreement with the simulation as far as reflectivity and transmissivity are concerned. Moreover, measurements of group delay in reflection have been made for the the second grating shown in Fig. 6.1-(b). A perfect agreement with the simulation has been observed for this spectral function with maximum fluctuation of $\sim 18\,\text{ps}$ and RMS group delay ripple of $\sim 5\,\text{ps}$ within the 1 dB reflection bandwidth.

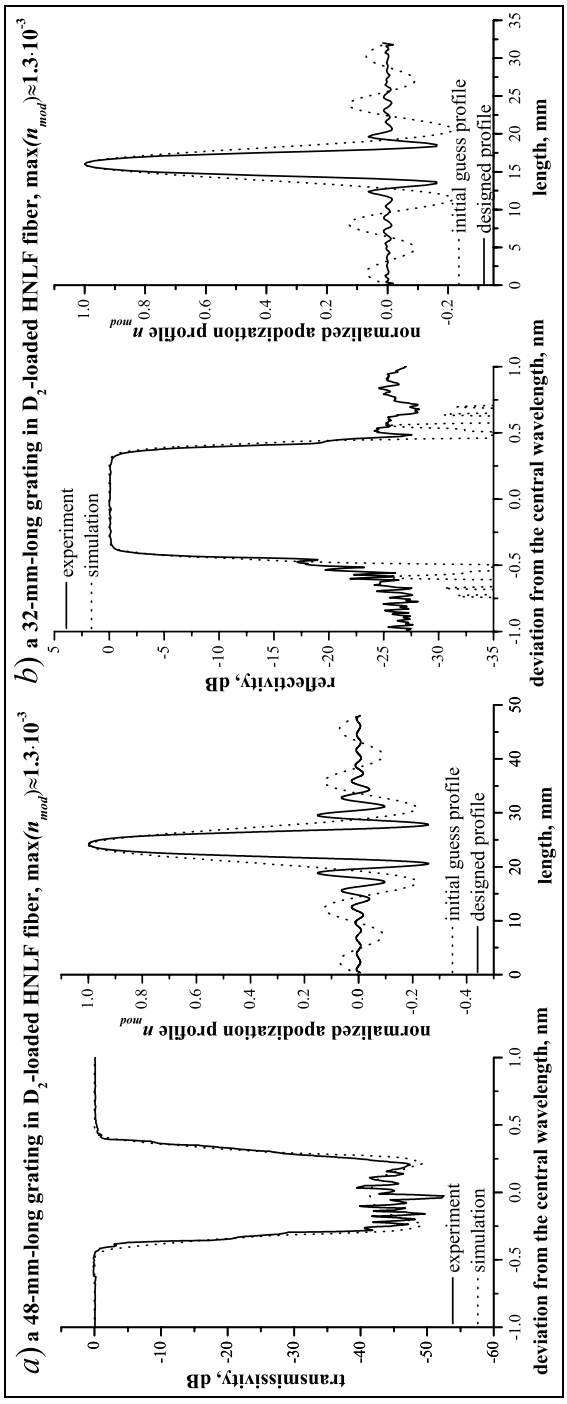

Figure 6.1: *(a) A 48-mm-long grating with its simulated (dotted) and measured (solid) transmissivity and its apodization profiles, initially "guessed" (dotted) and finally fitted (solid). (b) A 32-mm-long grating with its simulated (dotted) and measured (solid) reflectivity and its "guessed" and fitted apodization profiles.*

Actually, there are no special reasons for making the above gratings symmetric with respect to their center. Nevertheless, the examples demonstrate the strength of the suggested design technique as well as the power of the polarization control method, since we can see a perfect agreement between the designed target spectra and the experimentally measured ones.

6.2 Multichannel grating design

The method can also be used as a tool for designing multichannel fiber Bragg gratings. There exists a design technique where an N-channel grating design can be obtained by a dephasing approach, where the slowly varying envelope of a direct summation of N identical gratings, equally spaced in frequency space, is taken with different phases ϕ_i for each one-channel (*seeding*) grating [110,111]. One can expect that the *Marquardt algorithm* can be used here to find the optimal set of values ϕ_i to minimize the necessary maximum index change and to design the refractive index profile of a seeding grating as well as for fine-tuning of spectral qualities of the final multichannel grating profile.

It is though possible to design multichannel grating by direct use of the Marquardt algorithm. An example in Fig. 6.2 shows a 45 mm long multichannel grating designed to have three equidistant channels each being 0.23 nm wide with 30 dB side-lobe suppression and zero dispersion. The number of uniform subdivisions of the grating is $N = 250$ with the bandwidth of 5 nm subdivided into $M = 750$ intervals. The dotted line shows the initial profile which is a simple sinc function whose Fourier transform corresponds to the shape of a single channel of the grating. The solid line in this figure is the final zero-chirp apodization profile obtained after 30 iterations. In Fig. 6.3 one can see the spectrum of the designed grating which is in good agreement with the target spectrum. It has three distinct channels with 30 dB side lobe suppression and a group delay ripple of about 1 ps within the 1 dB reflection band of each channel.

6.3 Dispersion free gratings

Dispersion-free Bragg gratings play an important role in optical communication [83,112]. And the *Marquardt method* proves to be an efficient tool of their design. As an example, we consider a zero-chirp grating designed to be 45 mm long and to have a rectangular reflectivity profile with 30 dB side lobe suppression as well as zero dispersion in reflection within the 1 dB reflection band (or constant group delay). The number N of grating subdivisions was taken to be 120, and the number M of the points along the spectrum is 500.

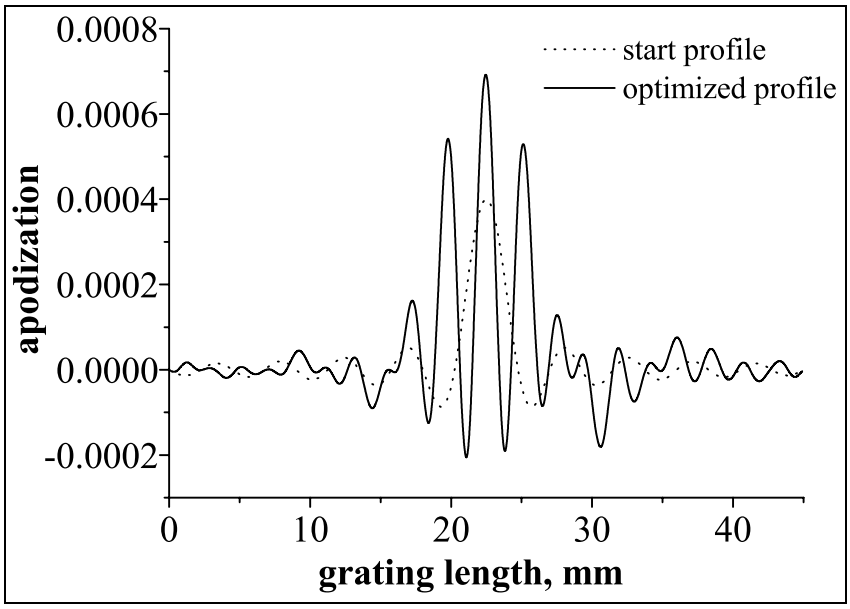

Figure 6.2: *Spectrum of the final optimized single-channel design.*

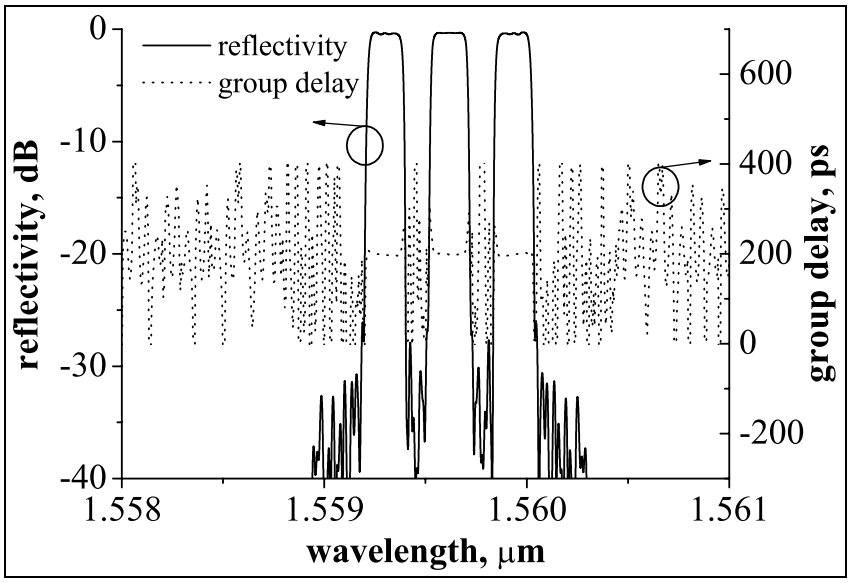

Figure 6.3: *Initial and final apodization profiles of a three-channel grating.*

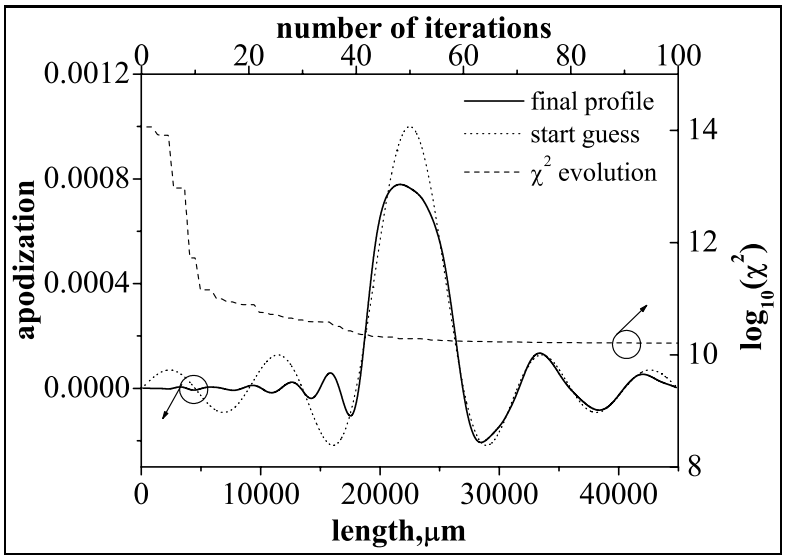

Figure 6.4: *Initial and final apodization profiles (a dotted and a solid line/left-bottom) of a single-channel grating and χ^2 evolution during the optimization process (a dashed line/right-top).*

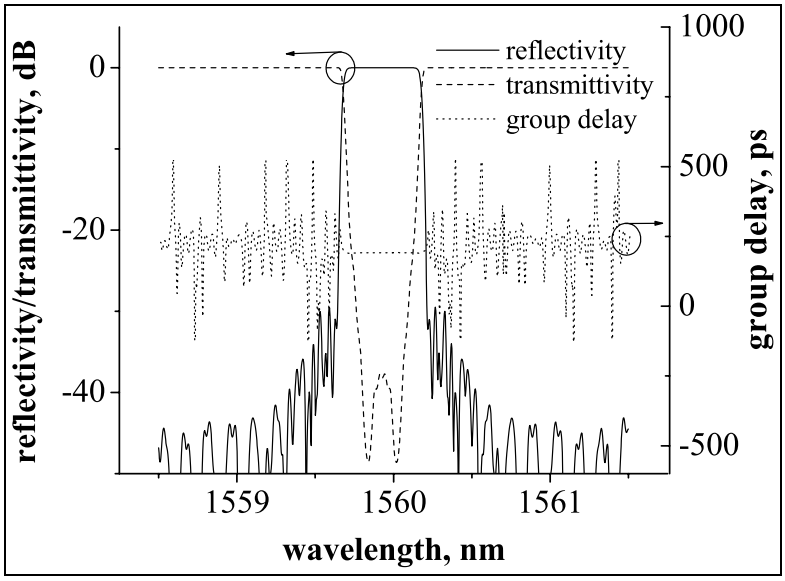

Figure 6.5: *Spectrum of the final optimized single-channel design.*

In Fig. 6.4 we can see the initial guess of the apodization profile shown as a dotted line and the final optimized apodization profile as a solid line (the left-bottom scale). The dependency of χ^2 as a function of the number of iterations can be seen in the same figure as a dashed line (the right-top scale). One can see that the number of iterations necessary to make in order to find the final solution is about 50. This makes the procedure very quick because the method has a quadratic convergence in the vicinity of the final solution. A typical run takes only a few minutes of CPU time for an average personal computer. As shown in Fig. 6.5 the spectral characteristics of the designed grating are in perfect agreement with the requirements that we had in the beginning of the iteration process. The value of the group-delay ripple is calculated by the simulation program to be $0.1\,\mathrm{ps}$. The commercially available software IFO_Gratings from Optiwave Corpotation [113] gives the same result.

6.4 Chirped gratings

Linearly chirped gratings play an important role in optical communication as dispersion compensators [114–121]. An appropriate choice of the apodization has a critical importance for short gratings [115]. We have not

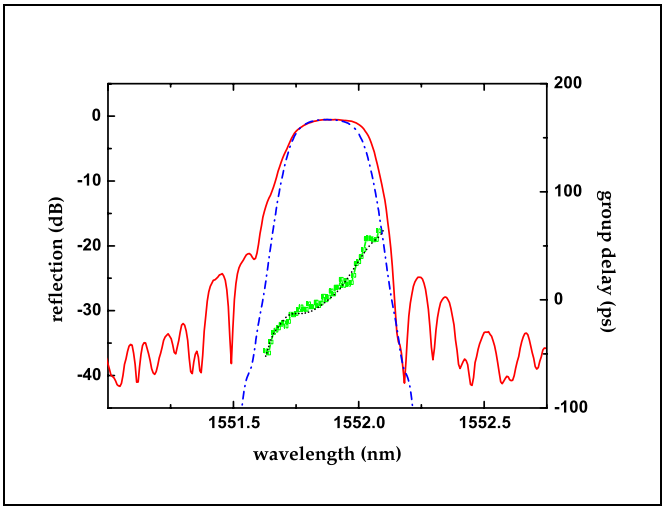

Figure 6.6: *Experimental (solid curve) and theoretical (dashed curve) reflection spectra, and measured (points) and simulated (dotted line) group delay for a 20 mm long chirped Gaussian grating. The peak reflectivity is 93%.*

implemented the Marquardt method for chirped gratings design. Such an implementation requires just some extra programming work without changing any principal ideas of the method. One would need to vary both apodization strength and average refractive index of the grating in order to get chirped grating designs. Nevertheless, my college H.-J. Deyerl wrote a few chirped grating using our polarization control method. A Gaussian apodization profile for the demonstration of a linearly chirped FBG for dispersion compensation has been chosen [78]. In Fig. 6.6 the reflection spectrum and the group delay are shown for a Gaussian apodized grating with length of $L = 20\,\text{mm}$, $s = 0.4$ and $\Lambda_{\text{mask}} = 1070.10\,\text{nm}$, using a linearly chirped phase mask of $0.212\,\text{nm/cm}$. The simulated group delay is in good agreement with the measured one and shows a dispersion of $200\,\text{ps/nm}$ and a RMS-group delay ripple of $6\,\text{ps}$.

6.5 Experimentally induced low-dispersion grating

This section presents one more low-dispersion grating that has been experimentally induced in HNLF fiber using the *polarization control method*. It was designed to be 23 mm long, to have a rectangular-shaped reflectivity profile and to have a constant group delay (zero dispersion) within the $-1\,\text{dB}$ reflection bandwidth. The number of uniform parts along the grating's length was taken to be 125, and the number of spectrum subdivisions was 750. The initial "guessed" and final optimized apodization profiles are shown in Fig. 6.7.

The designed grating has been induced experimentally in HNLF fiber. The simulated and experimentally measured curves for its transmittivity and reflectivity are shown in Fig. 6.9. The dotted lines represent simulation, while the solid ones show experimentally measured data. The graphs show an excellent agreement between the theoretical spectrum of the designed grating and the experimentally measured spectrum of the induced grating.

The group delay was measured by the *phaseshift method* [122, 123] and *RF modulation technique* [124] at a modulation frequency of 500 MHz, 1 GHz and 5 GHz as shown in Fig. 6.8. Using this technique, we measure a certain phase difference $\Delta\psi$ which can be converted to the group delay τ according to the following equation:

$$\Delta\psi = -2\pi f_m \tau, \tag{6.5-1}$$

where f_m is the used modulation frequency.

The theoretically predicted value of the group delay ripple at the -1 dB reflectivity level is equal to $0.05\,\text{ps}$. The measured value of the group-delay ripple with modulation frequency of 500 MHz is though equal to $\sim 0.6\,\text{ps}$. Nevertheless, the achieved experimental value of the group delay ripple can be considered to be satisfactory. As simulation results show, the phase characteristics of the grating are much more sensitive to the alignment of the experimental

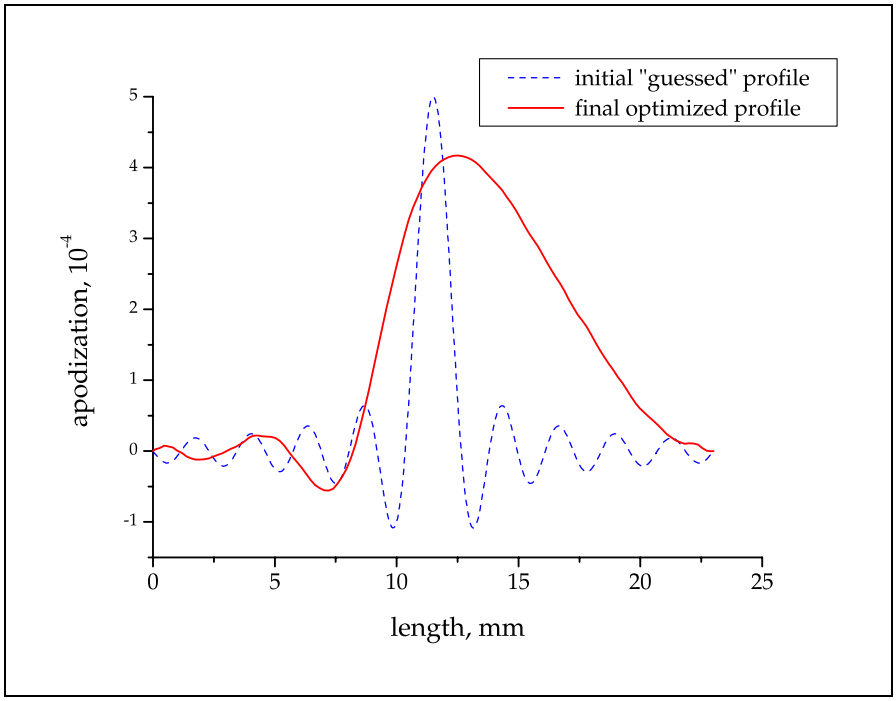

Figure 6.7: *Initial (dotted line) and final optimized (solid line) apodization profiles for a low dispersion rectangular-shaped grating.*

setup than its amplitude spectral functions such as reflectivity and transmittivity. Moreover, a much better result can be expected from a more stable UV laser source than the used KrF excimer laser. Our group is now in the progress of implementing the polarization control method using a 266 nm cw UV laser with a very stable power output ($< 1\%$), and we expect to be able to write gratings with much better spectral phase characteristics.

6.6 Gaussian-apodized gratings

Gaussian-apodized gratings with apodization profiles given by equation (4.2-20) provide strong side lobe suppression in the grating's spectrum [125]. Fig. 6.10 shows two gaussian-apodized gratings inscribed in deuterium loaded HNLF fiber using the polarization control method.

The grating in Fig. 6.10-(a) is a weak grating with $\sim 90\%$ peak reflectivity, modulation depth of $1.7 \cdot 10^{-4}$, length of 23 mm and taper parameter $g = 0.40$.

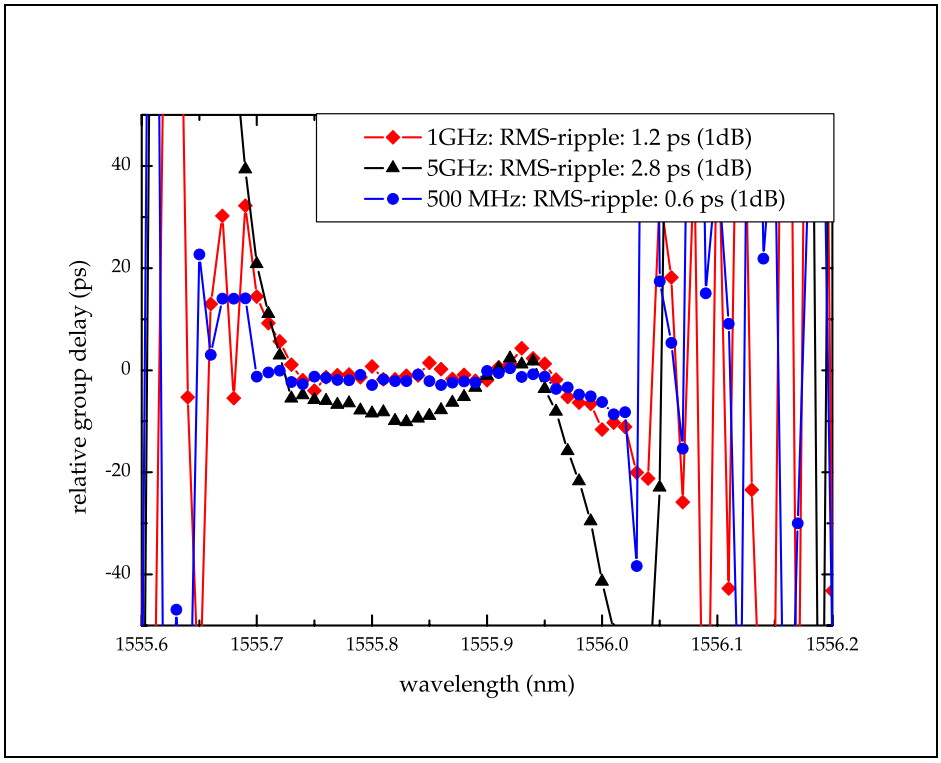

Figure 6.8: *Group delay measurements for a low-dispersion grating.*

Grating Fig. 6.10-(b) shows the transmittivity spectrum of an ultra strong Gaussian apodized grating with a measured transmittivity dip of $\sim 80\,\mathrm{dB}$ and a theoretical one of $\sim 100\,\mathrm{dB}$. It is 23 mm long too and has modulation depth of $1.4 \cdot 10^{-3}$. In both cases we have excellent agreement between the theory and the experiment. Some discrepancy between the simulation and the experiment in the case of the ultra strong is explained by the fact that no equipment can measure peak reflectivity of 100 dB beginning to operate at its noise level approximately at 70 dB. Strong Gaussian apodized gratings can be used as extinction (notch) filters, to cut out unwanted light for example from a pump laser.

These two examples show, that the polarization control method is capable of writing standard and compact apodization profiles in just one scan with side lobe suppressions up to 32.5 dB and a reflectivity up to almost 100%.

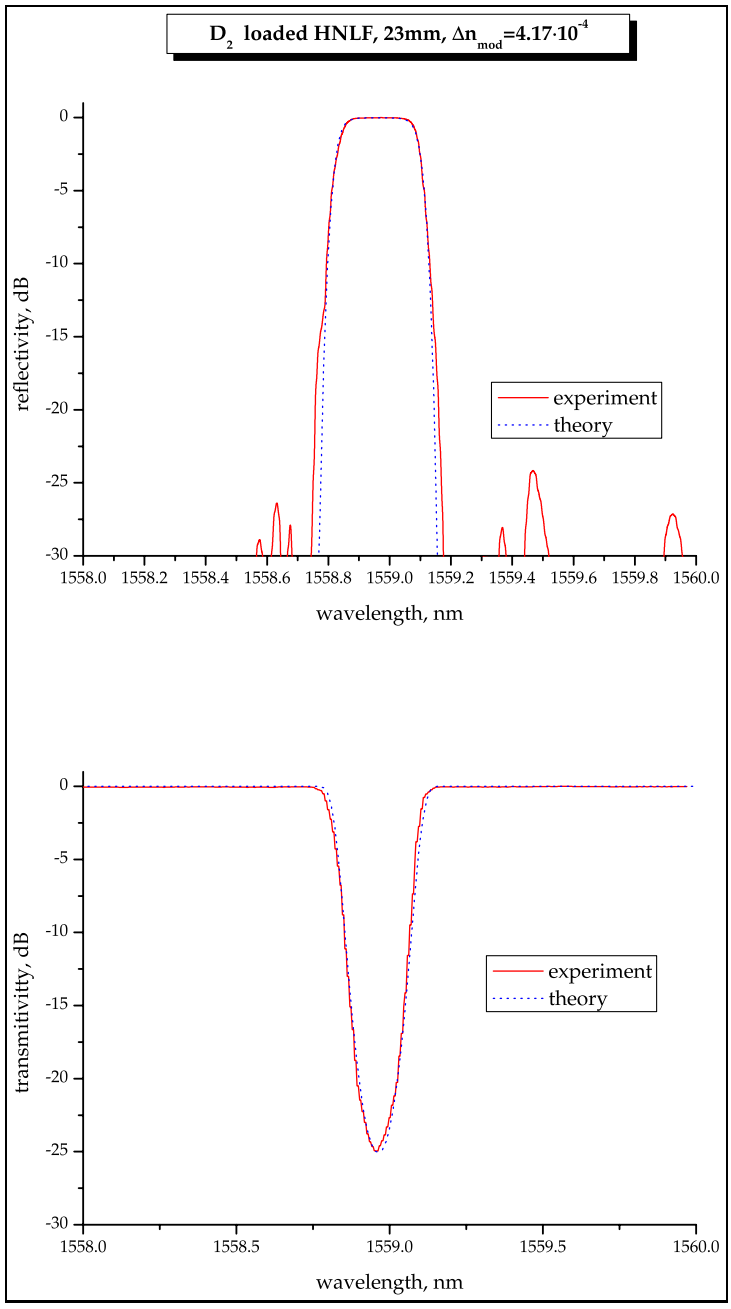

Figure 6.9: *Transmittivity and reflectivity curves for a low dispersion grating written in the HNLF fiber.*

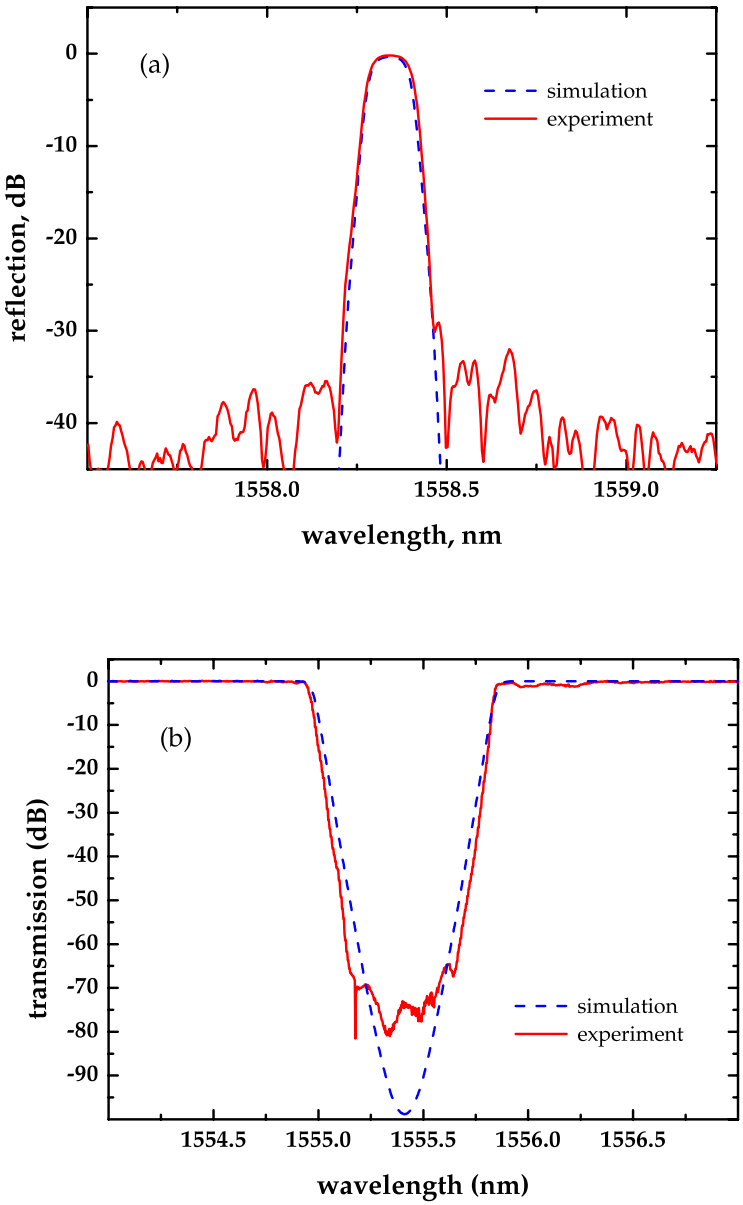

Figure 6.10: *(a) Experimental (solid curve) and theoretical (dashed curve) reflection spectra for of 23 mm long Gaussian apodized-grating. The peak reflectivity is 90%. (b) Experimental (solid curve) and theoretical (dashed curve) transmission spectra of a 23 mm long Gaussian apodized ultra strong grating with practically 100% peak reflectivity.*

Conclusion

As a conclusion, I would to summarize my Ph.D. project by mentioning once more my two main contributions to the fields of UV photosensitivity and Bragg gratings during the three years at COM, DTU. They are mentioned in the abstract of this thesis as well.

- ✘ Development of a novel polarization control method for UV writing of advanced Bragg gratings with arbitrary refractive index modulation profile including multiple π phase shifts. This method represents a practical cost-efficient technique that allows inscribing Bragg grating with any arbitrary apodization profile.
- ✘ Development of a novel efficient technique for Bragg grating design. The technique allows calculating an index modulation profile that should be inscribed in an optical fiber (or any other waveguide) in order to achieve a desired target spectrum of the grating. It is based on Marquardt-Levenberg algorithm of least-square optimization. The developed technique wins over all existing methods in computer time necessary for its implementation. Even more importantly, it has the remarkable ability to restrict some of the characteristics of the target grating, thus enabling, for example, the design of chirp-free gratings that are easy and cheap to fabricate with existing techniques, including the above mentioned polarization control method. In contrast, most other existing techniques produce complex grating designs with complicated chirp characteristics that are difficult, expensive and sometimes impossible to fabricate.

The experimental results presented in this Ph.D. thesis show high efficiency of the two techniques mentioned above. The *Levenberg-Marquardt method* is capable of designing simple apodization profiles that can be easily fabricated with the implemented *polarization control method*. Combined together, they provide an efficient tool to design and inscribe Bragg gratings with desired spectral specifications.

Acknowledgment

I would like to thank Technical University of Denmark for an opportunity to write a Ph.D. thesis at COM, as well as my supervisor Martin Kristensen for fruitful discussions and help during the four years of my Master's and Ph.D. studies.

I would also like to thank my colleges Hans-Jürgen Deyerl and Henrik Rokkjær Sørensen for effective and enjoyable work together. Now, finishing my Ph.D. project and leaving the field where I have worked for the last four years, I wish all who continue working with UV photosensitivity and Bragg gratings good luck in their interesting research.

Bibliography

[1] K.O. Hill, Y. Fujii, D.C. Johnson, and B.S. Kawasaki. Photosensitivity in optical waveguides; application to reflection filter fabrication. *Applied Physics Letters*, 32:647–649, 1978.

[2] I. Bennion, J.A.R. Williams, L. Zhang, K. Sugden, and N.J. Doran. UV-written in-fibre Bragg gratings. *Optical and Quantum Electronics*, 28(2):93–135, 1996.

[3] A. Othonos and K. Kalli. *Fiber Bragg gratings : Fundamentals and applications in telecommunications and sensing*. Artech House, Boston, 1999.

[4] R. Kashyap. *Fiber Bragg gratings*. Academic Press, San Diego, CA, 1999.

[5] M.O. Berendt. *Gratings in passive and active optical waveguides*. PhD thesis, COM, Technical University of Denmark, Kgs. Lyngby, 1999.

[6] M. Svalgaard. *Ultraviolet light induced refractive index structures in germanosilica*. PhD thesis, COM, Technical University of Denmark, Kgs. Lyngby, 2000.

[7] J. Hübner. *Index engineering with excimer light*. PhD thesis, COM, Technical University of Denmark, Kgs. Lyngby, 1998.

[8] B. Malo, S. Thériault, D.C. Johnson, F. Bilodeau, J. Albert, and K.O. Hill. Apodised in-fibre Bragg grating reflectors photoimprinted using a phase mask. *Electronics Letters*, 31(3):223–225, 1995.

[9] I. Riant. Fiber bragg gratings for optical telecommunications. *Comptes Rendus Physique*, 4(1):41–49, 2003.

[10] G. Nykolak, B.J. Eggleton, G. Lenz, and T.A. Strasser. Dispersion penalty measurements of narrow fiber bragg gratings at 10 Gb/s. *IEEE Photonics Technology Letters*, 10(9):1319–1321, 1998.

[11] B. Malo, J. Albert, F. Bilodeau, T. Kitagawa, D.C. Johnson, K.O. Hill, K. Hattori, Y. Hibino, and S. Gujrathi. Photosensitivity in phosphorus-doped silica glass and optical waveguides. *Applied Physics Letters*, 65:394–396, 1994.

[12] J.M. Senior. *Optical fiber communications. Principles and practice*. Prentice Hall, 1992.

[13] B.E.A. Saleh and M.C. Teich. *Fundamentals of Photonics*. John Wiley & Sons, Inc., New York, 1991.

[14] G. Meltz, W.W. Morey, and W.H. Glenn. Formation of bragg gratings in optical fibers by a transverse holographic method. *Optics Letters*, 14:823–825, 1989.

[15] W.W. Morey, G. Meltz, and W.H. Glenn. Holographically generated gratings in optical fibers. *Optics and Photonics News*, 1, 1994.

[16] H. Hosono, Y. Abe, D.L. Kinser, R.A. Weeks, K. Muta, and H. Kawazoe. Nature and origin of the 5-eV band in $SiO_2 : GeO_2$ glasses. *Physical Review B (Condensed Matter)*, 46(18):11445–11451, 1992.

[17] M. Fujimaki, T. Watanabe, T. Katoh, T. Kasahara, N. Miyazaki, Y. Ohki, and H. Nishikawa. Structures and generation mechanisms of paramagnetic centers and absorption bands responsible for Ge-doped SiO_2 optical-fiber gratings. *Physical Review B (Condensed Matter)*, 57(7):3920–3926, 1998.

[18] Linards Skuja. Optically active oxygen-deficiency-related centers in amorphous silicon dioxide. *Journal of Non-Crystalline Solids*, 239(1-3):16–48, 1998.

[19] J. Nishii, K. Kintaka, H. Hosono, H. Kawazoe, M. Kato, and K. Muta. Pair generation of ge electron centers and self-trapped hole centers in $GeO_2 – SiO_2$ glasses by KrF excimer-laser irradiation. *Physical Review B (Condensed Matter)*, 60(10):7166–7169, 1999.

[20] L. Skuja, M. Hirano, and H. Hosono. Oxygen-related intrinsic defects in glassy SiO_2: interstitial ozone molecules. *Physical Review Letters*, 84(2):302–305, 2000.

[21] M.G. Sceats, G.R. Atkins, and S.B. Poole. Photolytic index changes in optical fibers. *Annual Review of Material Science and Annual Review of Materials Science*, 23:381–410, 1993.

[22] H.G. Limberger, P.-Y. Fonjallaz, R.P. Salathe, and F. Cochet. Compaction- and photoelastic-induced index changes in fiber Bragg gratings. *Applied Physics Letters*, 68(22):3069–3071, 1996.

[23] M. Douay, W.X. Xie, T. Taunay, P. Bernage, P. Niay, P. Cordier, B. Poumellec, L. Dong, J.F. Bayon, H. Poignant, and E. Delevaque. Densification

involved in the UV-based photosensitivity of silica glasses and optical fibers. *Lightwave Technology, Journal of*, 15(8):1329–1342, 1997.

[24] Fan Piao, William G. Oldham, and Eugene E. Haller. The mechanism of radiation-induced compaction in vitreous silica. *Journal of Non-Crystalline Solids*, 276(1-3):61–71, 2000.

[25] H. Scholze. *Glass: nature and structure of glass*. Springer, 1990.

[26] M.J. Yuen. Ultraviolet absorption studies of germanium silicate glasses. *Applied Optics*, 21(1):136–140, 1982.

[27] Tsung-Ein Tsai, Glen M. Williams, and E. Joseph Friebele. Index structure of fiber Bragg gratings in $Ge - SiO_2$ fibers. *Optics Letters*, 22(4):224–226, 1997.

[28] V. Grubsky, D.S. Starodubov, and J. Feinberg. Photochemical reaction of hydrogen with germanosilicate glass initiated by 3.4-5.4 eV ultraviolet light. *Optics Letters*, 24(11):729–731, 1999.

[29] M.J.F. Digonnet. A Kramers-Kronig analysis of the absorption change in fiber gratings. *Proceedings of the SPIE - The International Society for Optical Engineering*, 2841:109–120, 1996.

[30] M. Kristensen. Ultraviolet-light-induced processes in germanium-doped silica. *Physical Review B (Condensed Matter and Materials Physics)*, 64(14):144201/1–12, 2001.

[31] M. Kristensen. *Refractive index engineering in silica glasses*. COM, DTU, Kongens Lyngby, Denmark, 2003.

[32] M. Hüfner. *Optical spectra of transparent rare earth compounds*. Academic Press, New York, 1978.

[33] R. Reisfeld and C. K. Jørgensen. *Lasers and excited states of rare earths*. Springer, Berlin, 1977.

[34] V.B. Sulimov, V.O. Sokolov, E.M. Dianov, and B. Poumellec. Photoinduced structural transformation in silica glass: the role of oxygen vacancies in the mechanism for UV-written refractive index gratings. *Physica Status Solidi (A) Applied Research*, 158(1):155–160, 1996.

[35] G. Pacchioni and R. Ferrario. Optical transitions and EPR properties of two-coordinated Si, Ge, Sn and related H(I), H(II), and H(III) centers in pure and doped silica from ab initio calculations. *Physical Review B (Condensed Matter)*, 58(10):6090–6096, 1998.

[36] P.J. Lemaire, R.M. Atkins, V. Mizrahi, and W.A. Reed. High pressure H_2 loading as a technique for achieving ultrahigh UV photosensitivity and thermal sensitivity in GeO_2 doped optical fibres. *Electronics Letters*, 29(13):1191–1193, 1993.

[37] B.L. Zhang and K. Raghavachari. Microscopic reaction mechanisms in hydrogen-loaded germanosilicate fibers: formation of divalent Ge defects. *Physical Review B (Condensed Matter)*, 51(12):7946–7949, 1995.

[38] R.L. Mozzi and B.E. Warren. The structure of vitreous silica. *Journal of Applied Crystallography*, 2(4):164–172, 1969.

[39] J. Skaar. *Synthesis and characterization of fiber Bragg gratings*. PhD thesis, Institute of Physical Electronics, Trondheim, Norway, 2000.

[40] R. Syms and J. Cozens. *Optical guided waves and devices*. McGraw-Hill Book Company, London, 1992.

[41] A.W. Snyder and J.D. Love. *Optical waveguide theory*. Chapman and Hall, London, New York, 1983.

[42] G.P. Agrawal. *Nonlinear fiber optics*. Academic Press, San Diego, 2001.

[43] A.P. Prudnikov, Yu.A. Brychkov, and O.I. Marichev. *Integrals and series - Special functions*. Gordon & Breach, New York, 1992.

[44] T. Erdogan. Fiber grating spectra. *Journal of Lightwave Technology*, 15(8):1277–1294, 1997.

[45] L. Poladian. Resonance mode expansions and exact solutions for nonuniform gratings. *Physical Review E*, 54:2963–2975, 1996.

[46] J.E. Sipe, L. Poladian, and C.M. Sterke. Propagation through nonuniform grating structures. *Journal of the Optical Society of America - A*, 11:1307–1320, 1994.

[47] T. Hirono and Y. Yoshikuni. A hamiltonian formulation for coupled-wave equations. *IEEE Journal of Quantum Electronics*, 30(8):1751–1755, 1994.

[48] A. Yariv. Coupled-mode theory for guided-wave optics. *IEEE Journal of Quantum Electronics*, QE9(9):919–933, 1973.

[49] B. Crosignani, P. Di Porto, and A. Yariv. Coupled-mode theory and slowly-varying approximation in guided-wave optics. *Optics Communications*, 78(3-4):237–239, 1990.

[50] H. Kogelnik. Filter response of nonuniform almost-periodic structures. *Bell System Technical Journal*, 55(1):109–126, 1976.

[51] L.A. Weller-Brophy and D.G. Hall. Analysis of waveguide gratings: a comparison of the results of Rouard's method and coupled-mode theory. *Journal of the Optical Society of America A*, 4(1):60–65, 1987.

[52] H. Kogelnik. *Theory of optical waveguides, guided-wave optoelectronics*. Springer-Verlag, New York, 1990.

[53] L. Poladian. Group-delay reconstruction for fiber bragg gratings in reflection and transmission. *Optics Letters*, 22(20):1571–1573, 1997.

[54] H.G. Song. Theory of symmetry in optical filter responses. *Journal of the Optical Society of America A: Optics and Image Science, and Vision*, 11(7):2027–2037, 1994.

[55] L.A. Coldren and S.W. Corzine. *Diode lasers and photonic integrated circuits*. N.Y. Wiley, New York, 1995.

[56] R. Kashyap, A. Swanton, and D.J. Armes. Simple technique for apodising chirped and unchirped fibre Bragg gratings. *Electronics Letters*, 32(13):1226–1228, 1996.

[57] S.J. Mihailov, F. Bilodeau, K.O. Hill, D.C. Johnson, J. Albert, and A.S. Holmes. Apodization technique for fiber grating fabrication with a halftone transmission amplitude mask. *Applied Optics*, 39(21):3670–3677, 2000.

[58] J. Martin and F. Ouellette. Novel writing technique of long and highly reflective in-fibre gratings. *Electronics Letters*, 30(10):811–812, 1994.

[59] K. O. Hill, F. Bilodeau, B. Malo, T. Kitagawa, S. Thériault, D. C. Johnson, J. Albert, and K. Takiguchi. Aperiodic in-fiber bragg gratings for optical dispersion compensation. In *Postdeadline Papers, Conference on Optical Fiber Communication*, volume 4, page PD77, Washington, D. C., 1994. Optical Society of America.

[60] R. Stubbe, B. Sahlgren, S. Sandgren, and A. Asseh. Novel technique for writing long superstructured fiber bragg gratings. In *Photosensitivity and Quadratic Nonlinearity in Glass Waveguides: Fundamentals and Applications*, volume 22, page PD1, Washington, D. C., 1995. Optical Society of America.

[61] M.J. Cole, W.H. Loh, R.I. Laming, M.N. Zervas, and S. Barcelos. Moving fibre/phase mask-scanning beam technique for enhanced flexibility in

producing fibre gratings with uniform phase mask. *Electronics Letters*, 31(17):1488–1490, 1995.

[62] Kai-Ping Chuang, Yinchieh Lai, and Lih-Gen Sheu. Complex fiber grating structures fabricated by sequential writing with polarization control. *Optics Letters*, 29(4):340–342, 2004.

[63] J.B.D. Jensen, N. Plougmann, H.-J. Deyerl, P. Varming, J. Hübner, and M. Kristensen. Polarization control method for ultraviolet writing of advanced Bragg gratings. *Optics Letters*, 27(12):1004–1006, 2002.

[64] H.-J. Deyerl, N. Plougmann, F. Floreani, B. Zsigri, C. Peucheret, S.J. Hewlett, and M. Kristensen. A compact low dispersion fiber Bragg grating with high detuning tolerance for advanced modulation formats. *Optics Communication*, 2004. (Submitted).

[65] M. Kristensen, J. Arentoft, J.B.D. Jensen, H.-J. Deyerl, J. Lægsgaard, C.-J. Marckmann, N. Plougmann, Y. Ren, S. Søgaard, and P. Varming. Bragg gratings and poling. *DOPS-NYT*, 16(2):49–54, 2001.

[66] P. Varming, J.B.D. Jensen, N. Plougmann, M. Kristensen, and J. Hübner. New method for fabrication of advanced UV written Bragg gratings. In *BGPP 2001, paper BWA5*, Stresa, Italy, 2001.

[67] H.-J. Deyerl, N. Plougmann, J.B.D. Jensen, J. El-Bez, H.R. Sørensen, C. Peucheret, and M. Kristensen. Low-dispersion fiber Bragg gratings written using the polarization control method. In *ECOC, paper 7.2.7*, Copenhagen, Denmark, 2002.

[68] H.-J. Deyerl, N. Plougmann, J.B.D. Jensen, H.R. Sørensen, and M. Kristensen. Polarization control method for UV writing of advanced Bragg gratings. In *IEEE/LEOS WFOPC*, pages 86–91, Glasgow, Scotland, 2002.

[69] J.B.D. Jensen, N. Plougmann, H.-J. Deyerl, and M. Kristensen. Polarization controlled UV writing of Bragg gratings. In *OFC, paper TuQ4*, pages 111–113, Anaheim, California, USA, 2002.

[70] N. Plougmann, J.B.D. Jensen, H.-J. Deyerl, H.R. Sørensen, and M. Kristensen. Polarization controlled UV writing of Bragg gratings. In *POWAG, paper WA3*, St. Petersburg, 2002.

[71] H.-J. Deyerl, H.R. Sørensen, J.B.D. Jensen, N. Plougmann, and M. Kristensen. Fabrication and stability of fiber Bragg gratings for WDM applications using a 266 nm cw-laser. In *CLEO/QELS, paper CtuI2*, Baltimore, Maryland, USA, 2003.

[72] F. Floreani, H.-J. Deyerl, N. Plougmann, H. Ou, J.B.D. Jensen, and M. Kristensen. A flexible approach for the apodization of planar waveguide Bragg gratings. In *BGPP, paper MD15*, Monterey, California, USA, 2003.

[73] N. Plougmann. Advanced techniques for fabricating Bragg gratings. Master's thesis, COM, Technical University of Denmark, Kgs. Lyngby, 2001.

[74] J.B.D. Jensen. *UV writing of advanced Bragg gratings in optical waveguides*. PhD thesis, COM, Technical University of Denmark, Kgs. Lyngby, 2002.

[75] H.R. Sørensen. UV-written advanved Bragg gratings in optical waveguides using a 266 nm cw laser. Master's thesis, COM, Technical University of Denmark, Kgs. Lyngby, 2003.

[76] C. Zhang. Polarization controlled UV-writing of Bragg gratings in fibers. Master's thesis, COM, Technical University of Denmark, Kgs. Lyngby, 2002.

[77] Mo Wu and Wenfeng Wang. UV writing of advanced Bragg gratings using polarization control method, 2003. (Three-week course supervised by Nikolai Plougmann).

[78] H.-J. Deyerl, N. Plougmann, J.B.D. Jensen, F. Floreani, H.R. Sørensen, and M. Kristensen. Fabrication of advanced Bragg gratings with complex apodization profiles using the polarization control method. *Applied Optics - LP*, 2003. (Accepted March 2004).

[79] E. Dalsgaard, T. Skettrup, and M. Owner-Petersen. *Optoelektronik (optiske komponenter)*. Polyteknisk Forlag, DTU, 1987.

[80] P.M. Petersen and T. Skettrup. *Ulineær optik*. Polyteknisk Forlag, DTU, 1994.

[81] D.K. Cheng. *Fundamentals of engineering electromagnetics*. Addison-Wesley, 1993.

[82] *Properties of Silicon*. INSPEC. The institution of electrical engineers, 1998.

[83] M. Ibsen, M.K. Durkin, M.J. Cole, and R.I. Laming. Optimised square passband fibre bragg grating filter with in-band flat group delay response. *Electronics Letters*, 34(8):800–802, 1998.

[84] Qian Yujun. *Optical fiber lasers*. PhD thesis, COM, Technical University of Denmark, Kgs. Lyngby, 2000.

[85] N. Plougmann. Advanced techniques for fabricating Bragg gratings. Master's thesis, COM, Technical University of Denmark, Kgs. Lyngby, 2001.

[86] M. Parent, J. Bures, S. Lacroix, and J. Lapierre. Polarising properties of reflecting Bragg filters induced by photosensitisation in monomode optical fibers. *Applied Optics*, 24(3):354–357, 1985.

[87] P. Niay, P. Bernage, T. Taunay, M. Douay, E. Delevaque, S. Boj, and B. Poumellec. Polarization selectivity of gratings written in Hi-Bi fibers by the external method. *IEEE Photonics Technology Letters*, 7(4):391–393, 1995.

[88] J.L. Philipsen, M.O. Berendt, P. Varming, V.C. Lauridsen, J.H. Povlsen, J. Hübner, M. Kristensen, and B. Pàlsdòttir. Polarisation control of DFB fibre laser using UV-induced birefringent phase-shift. *Electronics Letters*, 34(7):678–679, 1998.

[89] Ashish M. Vengsarkar, Qian Zhong, Daryl Inniss, W.A. Reed, Paul J. Lemaire, and S.G. Kosinski. Birefringence reduction in side-written photoinduced fiber devices by a dual-exposure method. *Optics Letters*, 19(16):1260–1262, 1994.

[90] M. Janos, J. Canning, and M.G. Sceats. Incoherent scattering losses in optical fiber Bragg gratings. *Optics Letters*, 21(22):1827–1829, 1996.

[91] T. Erdogan and V. Mizrahi. Characterization of UV-induced birefringence in photosensitive Ge-doped silica optical fibers. *Journal of the Optical Society of America B (Optical Physics)*, 11(10):2100–2105, 1994.

[92] T. Meyer, P.-A. Nicati, P.A. Robert, D. Varelas, H.-G. Limberger, and R.P. Salathe. Reversibility of photoinduced birefringence in ultralow-birefringence fibers. *Optics Letters*, 21(20):1661–1663, 1996.

[93] M. Douay, W.X. Xie, T. Taunay, P. Bernage, P. Niay, P. Cordier, B. Poumellec, L. Dong, J.F. Bayon, H. Poignant, and E. Delevaque. Densification involved in the UV-based photosensitivity of silica glasses and optical fibers. *Lightwave Technology, Journal of*, 15(8):1329–1342, 1997.

[94] P. Niay, P. Bernage, B. Leconte, E. Delevaque, and H. Poignant. Does photosensitivity pave the way towards the fabrication of miniature coherent light sources in inorganic glass waveguides? *Optical Materials*, 11(2-3):115–129, 1999.

[95] L. Poladian. Iterative and noniterative design algorithms for Bragg gratings. *Optical Fiber Technology*, 5(2):215–222, 1999.

[96] J. Skaar, Ligang Wang, and T. Erdogan. On the synthesis of fiber Bragg gratings by layer peeling. *Quantum Electronics, IEEE Journal of*, 37(2):165–173, 2001.

[97] L. Wang and T. Erdogan. Layer peeling algorithm for reconstruction of long-period fibre gratings. *Electronics Letters*, 37(3):154–156, 2001.

[98] G.-H. Song and S.-Y. Shin. Design of corrugated waveguide filters by the Gel'fand-Levitan-Marchenko inverse-scattering method. *Journal of the Optical Society of America A (Optics and Image Science)*, 2(11):1905–1915, 1985.

[99] E. Peral, J. Capmany, and J. Marti. Design of fibre grating dispersion compensators using a novel iterative solution to the Gel'fand-Levitan-Marchenko coupled equations. *Electronics Letters*, 32(10):918–919, 1996.

[100] R. Feced, M.N. Zervas, and M.A. Muriel. An efficient inverse scattering algorithm for the design of nonuniform fiber Bragg gratings. *Quantum Electronics, IEEE Journal of*, 35(8):1105–1115, 1999.

[101] M.A. Muriel, J. Azaña, and A. Carballar. In *BGPP*, pages 250–251, Optical Society of America, Washington, D.C., USA, 1999.

[102] C.-L. Lee and Y. Lai. Evolutionary programming synthesis of advanced fiber grating devices. In *Proceedings of CLEO/QELS, paper CTuI5*, 2003.

[103] L. Poladian. Simple grating synthesis algorithm. *Optics Letters*, 25(11):787–789, 2000.

[104] A. Rosenthal and M. Horowitz. Inverse scattering algorithm for reconstructing strongly reflecting fiber Bragg gratings. *Quantum Electronics, IEEE Journal of*, 39(8):1018–1026, 2003.

[105] N. Plougmann, M. Kristensen, and H.-J. Deyerl. New iterative approach for designing Bragg gratings. In *BGPP, paper MD17*, Monterey, California, USA, 2003.

[106] N. Plougmann and M. Kristensen. Efficient iterative technique for designing Bragg gratings. *Optics Letters*, 29(1):23–25, 2004.

[107] W.H. Press, S.A. Teukovsky, W.T. Vetterling, and B.P. Flannery. *Numerical recipes in Fortran*, chapter 15.2. Cambridge University Press, Cambridge, New York, 1992.

[108] K. Levenberg. A method for the solution of certain non-linear problems in least squares. *Quarterly of Applied Mathematics*, 2:164–168, 1944.

[109] D.W. Marquardt. An algorithm for least-squares estimation of nonlinear parameters. *Journal of the Society for Industrial and Applied Mathematics*, 11(2):431–441, 1963.

[110] K.Y. Kolossovski, R.A. Sammut, A.V. Buryak, and D.Yu. Stepanov. Three-step design optimization for multi-channel fibre Bragg gratings. *Optics Express*, 11(9), 2003.

[111] A.V. Buryak, K.Y. Kolossovski, and D.Yu. Stepanov. Optimization of refractive index sampling for multichannel fiber bragg gratings. *Quantum Electronics, IEEE Journal of*, 39(1):91–98, 2003.

[112] G.P. Agrawal. *Fiber-optic communication systems, Wiley series in microwave and optical engineering*. John Wiley & Sons, Inc., 1997.

[113] Optiwave Corporation. *Integrated fiber optical gratings design software*. Ottawa, Canada, 2001. http://www.optiwave.com.

[114] B.J. Eggleton, A. Ahuja, P.S. Westbrook, J.A. Rogers, P. Kuo, T.N. Nielsen, and B. Mikkelsen. Integrated tunable fiber gratings for dispersion management in high-bit rate systems. *Lightwave Technology, Journal of*, 18(10):1418–1432, 2000.

[115] D. Pastor, J. Capmany, D. Ortega, V. Tatay, and J. Marti. Design of apodized linearly chirped fiber gratings for dispersion compensation. *Lightwave Technology, Journal of*, 14(11):2581–2588, 1996.

[116] K. Ennser, N. Zervas, and R.L. Laming. Optimization of apodized linearly chirped fiber gratings for optical communications. *Quantum Electronics, IEEE Journal of*, 34(5):770–778, 1998.

[117] Tom Stephens, John Arkwright, Kerry Hinton, Dmitrii Yu Stepanov, Peter A. Krug, Benedict Smith, George Dhosi, Gideon Yoffe, and Francois Ouellette. Fiber gratings for dispersion compensation. *Conference on Optical Fiber Communication, Technical Digest Series*, page 71, 1998.

[118] T. Stephens, J. Arkwright, D.Y. Stepanov, P.A. Krug, B. Smith, G. Dhosi, G. Yoffe, and F. Ouellette. Chirped bragg grating dispersion compensation. *Proceedings APCC'97. Third Asia-Pacific Conference on Communications. Incorporating. ACOFT (Australian Conference on Optical Fibre Technology). ATNAC (Australian Telecommunication Networks and Applications Conference)*, pages 1602–1605 vol.3, 1997.

[119] F. Ouellette, J.-F. Cliche, and S. Gagnon. All-fiber devices for chromatic dispersion compensation based on chirped distributed resonant coupling. *Lightwave Technology, Journal of*, 12(10):1728–1738, 1994.

[120] B.J. Eggleton, T. Stephens, P.A. Krug, G. Dhosi, Z. Brodzeli, and F. Ouellette. Dispersion compensation using a fibre grating in transmission. *Electronics Letters*, 32(17):1610–1611, 1996.

[121] F. Ouellette. Dispersion cancellation using linearly chirped bragg grating filters in optical waveguides. *Optics Letters*, 12(10):847–849, 1987.

[122] C. Caspar, H.-M. Foisel, C.v. Helmolt, B. Strebel, and Y. Sugaya. Comparison of the cascadability performance of different types of commercially available wavelength (de)multiplexers. *IEE Conference Publication*, (448):91–94, 1997.

[123] S. Ryu, Y. Horiuchi, and K. Mochizuki. Novel chromatic dispersion measurement method over continuous Gigahertz tuning range. *Lightwave Technology, Journal of*, 7(8):1177–1180, 1989.

[124] C. Peucheret, F. Liu, and R.J.S. Pedersen. Measurement of small dispersion values in optical components [WDM networks]. *Electronics Letters*, 35(5):409–411, 1999.

[125] P.S. Cross and H. Kogelnik. Sidelobe suppression in corrugated-waveguide filters. *Optics Letters*, 1(1):43–45, 1977.

Index

E

F

G

H

I

J

K

L

M

N

O

P

Q

R

S

T

U

V

W

Contents